

Design and synthesis of antivirals benzimidazoles and quinoxalines

Tawfeek H. Abdelhafez^a, Muhammad K.F. Khattab^b, Ahmed Temirak^b, Yasser M. Shaker^b, Sherifa M. Abu Bakr^b, Eman M. Abbas^b, Sarah M.H. Khairat^b, Mona A. Abdullaziz^b, Ahmed A. El Rashidi^b, Reham A. Mohamed-Ezzat^b, Shadia A. Galal^b, Passant E.I. Moustafa^c, Sally A. El Awdan^c, Hamed I. Ali^d, Wafaa I. El-Eraky^c, Mostafa K. El Awady^a, Hoda I. El Diwani^b

^aDepartment of Microbial Biotechnology, Biotechnology Research Institute, National Research Centre, Giza, ^bDepartment of Chemistry of Natural & Microbial Products, Institute of Pharmaceutical and Drug Industries Research, ^cDepartment of Pharmacology, Institute of Medical, National Research Centre, Cairo, Egypt, ^dDepartment of Pharmaceutical Sciences, Texas A&M University, Irma Lerma Rangel College of Pharmacy, Texas, USA

Correspondence to Hoda I. El Diwani, (Prof. Dr.) & Shadia A. Galal (Prof. Dr.), Department of Chemistry of Natural and Microbial Products, Institute of Pharmaceutical and Drug Industries Research, National Research Centre, El Buhouth Street, Dokki, PO Box 12622, Cairo, Egypt.
E-mail: heldiwani@gmail.com, heldiwany@hotmail.com, sh12galal@hotmail.com

Received: 19 January 2022

Revised: 18 March 2022

Accepted: 22 March 2022

Published: 21 July 2022

Egyptian Pharmaceutical Journal 2022, 21:249–271

Background

Chronic hepatitis C can cause serious, even deadly, health problems like cirrhosis and liver cancer. There is no vaccine for hepatitis C. The hepatitis C virus (HCV) NS5B gene encodes RNA-dependent RNA polymerase, which is a key player in viral replication and is a promising target for the development of antiviral drugs. Drugs having benzimidazole and quinoxaline scaffolds were described to selectively block the activity of NS5B polymerase. New antiviral drugs have to be developed to overcome drug resistance.

Objective

The main goal of this work was to develop new effective anti-bovine viral diarrhea virus (BVDV) and anti-HCV agents by designing and synthesizing benzimidazole and quinoxaline derivatives.

Materials and methods

Synthesis of target compounds based on benzimidazole and quinoxaline scaffolds according to reported methods was done. Antiviral activity against BVDV was studied. BVDV and Madin-Darby bovine kidney cells were obtained from the American Type Culture Collection. Antiviral activity against HCV infectious system was evaluated. Huh7.5.1 cells were cultured and treated with different concentrations of studied compounds. GOLD molecular docking study was evaluated. The crystal structures of the HCV polymerases in complex with its co-crystallized native ligand were retrieved from the Protein Data Bank. Acute toxicity studies were carried out on animals.

Results and conclusion

A rational design based on the previous work was performed to indicate new promising benzimidazole and quinoxaline derivatives to be synthesized and tested as anti-HCV compounds. New benzimidazole and quinoxaline derivatives were synthesized and tested for anti-BVDV activity. All of the compounds showed strong activity against BVDV, except **17**, which exhibited moderate antiviral activity. Compounds **12** and **13** were the most promising. The anti-HCV activity of **12** and **13** was investigated after infection of Huh 7.5.1 cells with HCV (JFH1). The IC₅₀ values of **12** and **13** were found to be 19.1 and 49.4 μM, respectively; their CC₅₀ values were 752.25 and 1480 μM, respectively; and their SI were calculated to be 39.3 for **12** and 30.03 for **13**. The assigned compounds were docked into the hepatitis-C virus polymerase enzyme (pdb: 3FRZ) using GOLD 5.2.2 docking program. They revealed GoldScore fitness activities of 69.78–80.71, which is comparable to the native 'PF-00868554' ligand as a potent HCV polymerase inhibitor. They are bound by up to three hydrogen bonds, mainly with aminoacids R422 and S476, as well as they were embedded into the two small hydrophobic pockets formed by amino acid residues including L419, M423, L482, and L497. The acute toxicity of compound **12** on rats was tested. No signs of toxicity, no deaths, and no significant changes were observed in the biochemical parameters of liver and kidneys.

Keywords:

anti-bovine viral diarrhea virus activity, anti-hepatitis C virus activity, benzimidazoles, design, quinoxalines

Egypt Pharmaceut J 21:249–271
© 2022 Egyptian Pharmaceutical Journal
1687-4315

Introduction

The WHO, 2014, has stated that worldwide more than 185 million people are infected with hepatitis C virus (HCV), and of these people, 350 000–500 000 die each

This is an open access journal, and articles are distributed under the terms of the Creative Commons Attribution-NonCommercial-ShareAlike 4.0 License, which allows others to remix, tweak, and build upon the work non-commercially, as long as appropriate credit is given and the new creations are licensed under the identical terms.

year. An estimated one-third of those who become chronically infected develop liver cirrhosis or hepatocellular carcinoma [1-5]. Furthermore, treatment remains unavailable for many who have been diagnosed.

HCV has a single-stranded positive-sense RNA genome that encodes a single polyprotein of ~3000 amino acids. It is divided into three structural proteins C, E1, and E2, responsible for building up the virus core and enveloping glycoproteins, and nonstructural proteins, p7, NS2, NS3, NS4A, NS4B, NS5A, and NS5B, responsible for supporting RNA replication [6].

Many direct-acting antivirals have been developed, including simeprevir [7] and sofosbuvir or sovaldi [8-10]. Sovaldi is a HCV nucleotide analog NS5B polymerase inhibitor indicated for the treatment of chronic hepatitis C infection as a component of a combination antiviral treatment regimen [2,11]. It can be used in combined therapy with the NS5A inhibitor ledipasvir or the NS5B non-nucleoside inhibitor GS-9669 against HCV genotype 1 infection [12]. When sovaldi is used in combination with ribavirin or peginterferon alfa/ribavirin, the contraindications applicable to those agents are applicable to combination therapies. Therapy using sofosbuvir and ribavirin has a few adverse effects such as fatigue and headache. Combined therapy of sofosbuvir-peginterferon and ribavirin possesses reported adverse effects, in addition to the ones mentioned before, nausea, insomnia, and anemia [13]. Moreover, there are certain subgroups of difficult-to-treat patients, especially those co-infected with HBV and HCV and subjected to high risk of hepatitis B reactivation. Some cases lead to fulminant hepatitis, hepatic failure, and death [14-16]. In addition, there are respiratory adverse effects associated with sofosbuvir regimens [17]. Treatment with direct-acting antivirals may lead to the emergence of resistant strains, does not protect from reinfection, and as infection is asymptomatic, people unaware of their status continue to transmit the virus [18]. New antivirals have to be developed to reach high genetic barriers to resistance. Combination of antivirals with different targets, each of them with high potency and high genetic barrier, can lead to successful therapy.

Numerous non-nucleoside inhibitors of the HCV polymerase have been reported [14]. Among these, a series that share a common benzimidazole scaffold [15-17] was described to selectively block the activity of NS5B polymerase [18,19], for example, JTK 109 (Japan Tobacco)(I) [12,17,20] and JTK003 [21] (II)

(Fig. 1). These inhibitors act as allosteric inhibitors and block the polymerase before elongation. JTK 109 was withdrawn from clinical trials for unknown reasons [22].

Quinoxaline 6-carboxylate pharmacophore bears good resemblance to the known benzimidazole 5-carboxylate NS5B RNA-dependent RNA polymerase inhibitor **III** ($IC_{50}=1.6 \mu M$) reported by Boehringer Ingelheim [23] (Fig. 1). The quinoxaline derivative **IV** (Fig. 1) shares the same structural feature of a bicyclic aromatic core substituted with two single cyclic groups at the left side and a carboxylate group at the right-hand side (Fig. 1) [23].

Bovine viral diarrhea virus (BVDV) is an enveloped member of the *Flaviviridae* family and a major pathogen for cattle. BVDV serves as the US EPA-approved surrogate for human hepatitis C because of the following: (a) the two viruses possess a high degree of genomic similarity; (b) their genomes code for functionally identical proteins that can serve as targets for inactivation; (c) both viruses are of similar size and both are enveloped, indicating similar susceptibility to disinfection; and (d) they establish persistent infections in their hosts at a similar frequency. BVDV is accepted by the US EPA as a surrogate for disinfectant efficacy testing against human HCV. A surrogate is necessary because HCV is difficult to propagate reproducibly in a cell culture [24,25].

The recent strategy for developing novel anti-HCV therapeutics aims at the identification of new anti-HCV modalities that are affordable by Egyptian patients and with minimal adverse effects and high recovery rate.

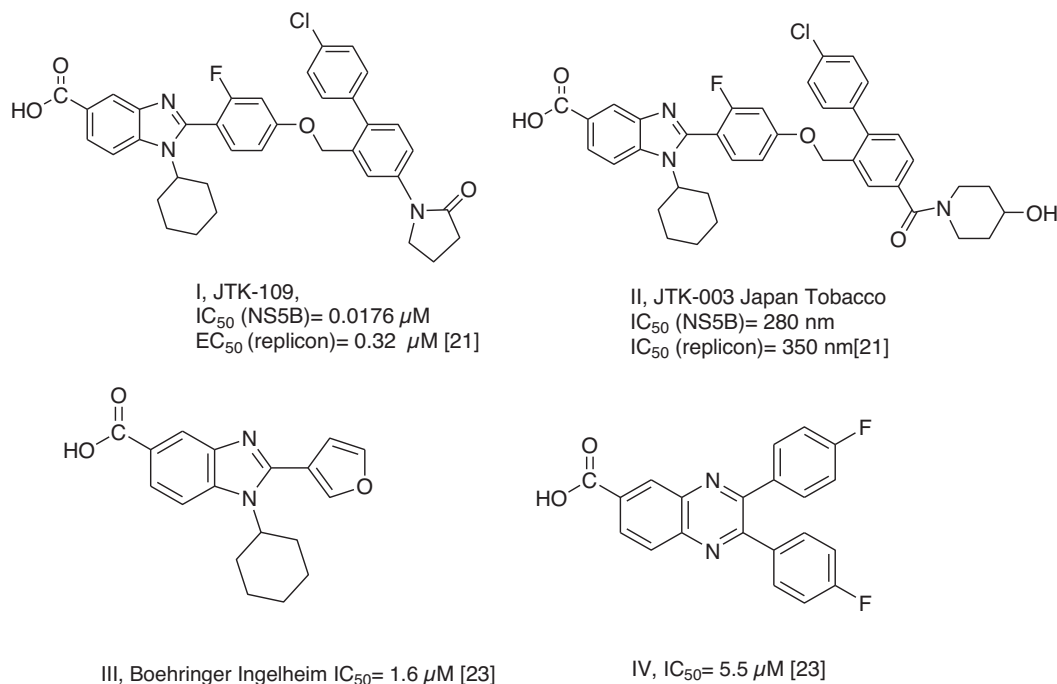
The main objective of this investigation was the development of novel potent anti-BVDV and anti-HCV agents by designing and synthesizing benzimidazole and quinoxaline derivatives through the introduction of effective substituents to the benzimidazole or quinoxaline scaffolds. Compound **12** was discovered to be an anti-HCV compound with $IC_{50}=19.1 \mu M$, $CC_{50}=752.25 \mu M$, $SI=39.3$, being nontoxic to rats, and has no significant changes in biochemical parameters of rats.

Materials and methods

General

Microanalyses of the spectral data of the compounds were performed in the Microanalytical laboratories,

Figure 1



Potent anti-HCV active agents have benzimidazole and quinoxaline scaffolds. HCV, hepatitis C virus.

National Research Centre, Cairo, Egypt. The IR spectra ($4000\text{--}400\text{ cm}^{-1}$) were recorded using KBr pellets in a Jasco FT/IR 300E Fourier transform infrared spectrophotometer on Perkin Elmer (Massachusetts, United States) FT-IR 1650 (spectrophotometer). The NMR spectra were recorded using Jeol (Germany) EX-270 MHz and 500 MHz NMR spectrophotometers. Chemical shifts are reported in parts per million (ppm) from the tetramethylsilane resonance in the indicated solvent. Coupling constants are reported in Hz; spectral splitting partners are designed as follows: singlet (s); doublet (d); triplet (t); and multiplet (m). The mass spectra were carried out using Finnigan mat SSQ 7000 (Thermo. Inst. Sys. Inc., (New Mexico, USA), spectroscopy at 70 eV. BVDV and Madin-Darby bovine kidney cells (MDBK) were obtained from American Type Culture Collection.

Chemistry

General procedure for the preparation of 12 or 13

A well-stirred solution of 2-(4-aminophenyl)-1H-benzimidazole **11** (10 mmol) [26] and sodium hydride (20 mmol) in dry dimethylformamide (DMF) was refluxed for half an hour, and then, benzenesulfonyl chloride (20 mmol) or 2-nitrobenzene-1-sulfonyl chloride (20 mmol) was added

dropwise. The reaction mixture was refluxed for 10 h and left to cool, poured into cold water, and neutralized with dil. HCl. The grayish solid was collected, washed with water, and dried to yield **12** or **13**, respectively.

N-(Benzenesulfonyl)-4-[1-(2-benzenesulfonyl)-1H-benzo[d]imidazol-2-yl]benzenamine (12)

Purification by chromatography column was achieved using the eluent ethyl acetate/pet. ether $60\text{--}80^\circ\text{C}$ in the ratio 3 : 1. $R_f=0.69$ (ethyl acetate : petroleum ether, 2 : 1), yield: 65%, m.p.: $255\text{--}258^\circ\text{C}$. IR (KBr) $\nu_{\text{max}}/\text{cm}^{-1}$: 3233 (NH aminophenyl); 3063, 2955, 2922 (CH arom); 1616 (C=N); 1566 (C=C arom); 1303 ($\nu_{\text{as}}\text{SO}_2$), 1090 ($\nu_{\text{s}}\text{SO}_2$). $^1\text{H-NMR}$ (DMSO- d_6 , 500 MHz, δ ppm): 7.27 (m, 2H); 7.37 (d, 2H, $J=7.65$ Hz); 7.48 (m, 2H, benzimidazole moiety); 7.55 (m, 4H, benzenesulfonyl moiety); 7.75 (m, 2H, benzimidazole moiety) 7.86 (m, 4H, benzenesulfonyl moiety); 8.02 (d, 2H, $J=7.65$ Hz); 11.04 (s, 1H, NH sulfonamide, D_2O exchangeable). $^{13}\text{C-NMR}$ (DMSO- d_6 , 500 MHz, δ ppm): 120.10, 122.60, 126.09, 127.23, 127.99, 128.08, 128.62, 129.92, 130.21, 133.65, 135.39 (aryl C=C), 139.75 (=C-S), 139.89 (=C-S), 151.27 (C=N). MS, m/z (%): 489 (M^+ , 38%). Anal. Calcd. for $\text{C}_{25}\text{H}_{19}\text{N}_3\text{O}_4\text{S}_2$ (489.08): C, 61.33; H, 3.91; N, 8.58; S, 13.10. Found: C, 61.30; H, 3.86; N, 8.54; S, 12.9.

N-(2-Nitrobenzenesulfonyl)-4-[1-(2-nitrobenzenesulfonyl)-1*H*-benzo[d]imidazol-2-yl]benzenamine (13)

$R_f=0.76$ (ethyl acetate/ pet. ether, 3 : 1), yield: 70%, m.p. more than 300°C. IR (KBr) $\nu_{\max}/\text{cm}^{-1}$: 3262 (NH aminophenyl); 3072, 2916, 2876 (CH arom); 1620 (C=N); 1546 (NO₂); 1377(NO₂), 1325(*vas*SO₂), 1091(*vs*SO₂). ¹H-NMR (DMSO-*d*₆, 500 MHz, δ ppm): 7.143(m, 2H), 7.46–7.49 (d, $J=8.8$ Hz, 2H), 7.59–7.62 (d, $J=8.8$ Hz, 2H), 7.71–8.057(m, 10H), 10.14(s, 1H, NH D₂O exchangeable). ¹³C-NMR (DMSO-*d*₆, 125 MHz, δ ppm): 120.0, 122.77, 122.93, 127.63, 128.22, 129.49, 130.59 (aryl C=C), 131.29 (=C-S) 139.72 (=C-S), 148.33 (=C-NO₂), 151.06 (C=N), 154.08 (=C-NO₂). Anal. Calcd. for C₂₅H₁₇N₅O₈S₂ (579.05): C, 51.81; H, 2.96; N, 12.08; S, 11.07. Found: C, 51.84; H, 2.99; N, 12.05; S, 11.10.

General procedure for the preparation 14–16

A mixture of the pyrazole derivatives **6a**, **6b**, **7**, and **8** [26,27] (10 mmol) and 2-(4-aminophenyl)-1*H*-benzimidazole derivatives **11** (10 mmol) in gl. acetic acid was refluxed for 8 h. The excess gl. acetic acid was evaporated under reduced pressure, and then the reaction mixture was poured into crushed ice with adding ammonia (two drops) to adjust pH 7. The formed solid was collected by vacuum filtration, dried, and recrystallized from ethanol.

4-(1*H*-Benzo[d]imidazol-2-yl)-*N*-[(3-methyl-1-phenyl-5-(4-phenylsulfonyl)piperazin-1-yl)-1*H*-pyrazol-4-yl)methylene]aniline (14)

$R_f=0.48$ (pet. ether/ethyl acetate, 1 : 3), yield=60%, m.p.: 236–237°C. IR (KBr) $\nu_{\max}/\text{cm}^{-1}$: 3495 (NH), 3157, 3111, 3059 (C=H), 2980, 2929 (C-H), 1670 (C=N), 1602 (C=C), 1546 (N-O stretch), 1371 (N-O stretch), 1325 (*vas* SO₂), 1125 (*vs* SO₂). ¹HMR (DMSO-*d*₆, 500 MHz, δ ppm): 2.032–2.067 (m, 4H, axial piperazinyl Hs), 2.47 (s, 3H, CH₃), 2.903–2.946 (m, 4H, equatorial piperazinyl Hs), 7.167 (dd, 2H), 7.4 (d, 2H, $J=7.65$ Hz); 7.44 (s, 1H, =CH), 7.52–7.8 (m, 10H), 7.90 (dd, 2H), 8.02 (d, $J=7.65$ Hz, 2H); 12.74(br, 1H, NH D₂O exchangeable). ¹³C NMR (DMSO-*d*₆, 500 MHz, δ ppm): 21.595, 24.657, 45 (piperazinyl C), 119.45, 122.51, 127.64, 13.62, (aryl C=C), 141.82 (=C-S), 151.16 (C=N). MS: m/z 601 (M⁺, 100%). Anal. Calcd. for C₃₄H₃₁N₇O₂S (601.23): C, 67.87; H, 5.19; N, 16.19; S, 5.33. Found C, 67.83; H, 5.17; N, 16.15; S, 5.39.

4-(1*H*-Benzo[d]imidazol-2-yl)-*N*-[(3-methyl-5-(4-(2-nitrophenylsulfonyl)piperazin-1-yl)-1-phenyl-1*H*-pyrazol-4-yl)methylene]aniline (15)

$R_f=0.26$ (pet. ether/ethyl acetate, 1 : 4), yield=50%, m.p.: 306°C. IR (KBr) $\nu_{\max}/\text{cm}^{-1}$: 3428 (NH), 3262, 3072 (C=H), 2916, 2876 (C-H), 1610 (C=N), 1546 (N-O stretch), 1355 (N-O stretch), 1320 (*vas* SO₂), 1128 (*vs* SO₂). ¹HNMR (DMSO-*d*₆, 500 MHz, δ ppm): 2.05 (m, 4H), 2.67 (s, 3H, CH₃), 2.9 (m, 4H), 7.14–7.18 (dd, 2H), 7.37 (d, $J=7.65$ Hz, 2H); 7.46–8.057 (m, 8H), 7.74 (s, 1H, CH=N), 7.92 (dd, 2H), 8.21 (m, 1H), 8.35 (d, $J=7.65$ Hz, 2H); 12.79 (s, 1H, NH, D₂O exchangeable). ¹³C NMR (DMSO-*d*₆) δ : 24.657, 45.794 (piperazinyl C), 119.477, 122.463, 125.162, 127.633 (aryl C=C), 141.33 (=C-S), 151.717 (C=N). MS: m/z 646 (M⁺, 100%). Anal. Calcd. for C₃₄H₃₀N₈O₄S (646.21): C, 63.14; H, 4.68; N, 17.33; S, 4.96. Found: C, 63.18; H, 4.74; N, 17.38; S, 5.12.

1-(4-(4-(4-(1*H*-Benzo[d]imidazol-2-yl)phenylimino)methyl)-3-methyl-1-phenyl-1*H*-pyrazol-5-yl)piperazin-1-yl)ethanone (16)

$R_f=0.25$ (ethyl acetate/pet. ether, 1 : 2), yield=64%, m.p.: 227–229°C. IR (KBr) $\nu_{\max}/\text{cm}^{-1}$: 3501 (NH), 1668 (C=O), 1601 (C=N), 1544, 1500 (C=C). ¹H NMR (DMSO-*d*₆, 500 MHz, δ ppm): 2.13–2.15 (m, 4H, axial piperazinyl Hs), 2.35 (s, 3H, CH₃), 2.48 (s, 3H, CH₃), 2.94–3.18 (m, 4H, equatorial piperazinyl Hs), 7.14–7.20 (dd, 2H), 7.30–7.33 (d, 2H, $J=7.65$ Hz), 7.41–7.50 (m, 5H), 7.59 (s, 1H, HC=N), 8.06–8.12 (dd, 2H, phenyl), 8.35 (d, 2H, $J=7.65$ Hz); 12.72 (s, 1H, NH, D₂O exchangeable). ¹³C NMR (DMSO-*d*₆, 500 MHz, δ ppm): 24.6, 24.6, 45.5 (piperazinyl C), 119.5, 122.2, 122.7, 127.6 (aryl C=C), 141.3 (=C-N), 151.7 (C=N), 169.1 (C=O). MS: m/z 503, (M⁺, 100%). Anal. Calcd. for C₃₀H₂₉N₇O (503.06): C, 71.55; H, 5.80; N, 19.47. Found C, 71.60; H, 5.83; N, 19.38.

4-(1*H*-Benzo[d]imidazol-2-yl)-*N*-[(3-methyl-1-phenyl-5-(piperidin-1-yl)-1*H*-pyrazol-4-yl)methylene]aniline (17)

$R_f=0.44$ (pet. ether/ethyl acetate, 3 : 1), yield=55%, m.p.: 102–105°C. IR (KBr) $\nu_{\max}/\text{cm}^{-1}$: 3400 (NH), 3191, 3066 (C=H), 2983, 2911 (C-H), 1621 (C=N). ¹H NMR (DMSO-*d*₆, 500 MHz, δ ppm): 1.70–1.94 (m, 6H), 2.18 (m, 4H), 2.47 (s, 3H, CH₃), 7.16–7.21 (dd, 2H), 7.29–7.32 (d, $J=7.65$ Hz, 2H), 7.41–7.50 (m, 5H), 7.56 (s, 1H, HC=N), 8.00–8.10 (dd, 2H, phenyl), 8.37 (d, $J=7.65$ Hz, 2H); 12.72 (s, 1H, NH, D₂O exchangeable). MS: m/z 460 (M⁺100%). Anal.

Calcd for C₂₉H₂₈N₆ (460.24): C, 75.63; H, 6.13; N, 18.25. Found: C, 75.69; H, 6.10; N, 18.19.

4-[(5-Chloro-3-methyl-1-phenyl-1H-pyrazol-4-yl)methyleneamino]benzoic acid (18)

To 4-aminobenzoic acid (10 mmol) in glacial acetic acid (30 ml), the pyrazole derivative **4** (10 mmol) was added. The reaction mixture was heated at 80°C for 24 h. The acetic acid was evaporated under vacuum, and the solid obtained was collected. $R_f=0.86$ (pet. ether/ethyl acetate, 1 : 1), yield =50%, m.p.: 158–160°C. ¹H NMR (DMSO-*d*₆, 500 MHz, δ ppm): 2.64 (s, 3H, CH₃), 7.36–7.41(m, 5H), 7.52 (d, $J=7.65$ Hz, 2H); 8.40 (d, $J=7.65$ Hz, 2H); 8.61 (s, 1H, N=CH), 11.36 (s, 1H, OH, D₂O exchangeable). MS: m/z 339 (M⁺, 100%). Anal. Calcd. for C₁₈H₁₄ClN₃O₂ (339.08): C, 63.63; H, 4.15; Cl, 10.43; N, 12.37; found C, 63.71; H, 4.25; Cl, 10.40; N, 12.44.

N-[(5-Chloro-3-methyl-1-phenyl-1H-pyrazol-4-yl)methylene]-4-(1-cyclohexyl-5-nitro-1H-benzo[d]imidazol-2-yl)benzenamine (20)

To compound **18** (10 mmol) in polyphosphoric acid (60 ml), compound **19** [28] (10 mmol) was added. The reaction mixture was gradually heated to 200°C, stirred for 4 h, allowed to cool to about 100°C, and poured in a large volume of rapidly stirred water. Ammonia solution was added until the solution was neutralized. The formed solid was collected, washed with water, dried, and the solid formed was recrystallized from acetic acid. $R_f=0.6$ (pet. ether/ethyl acetate, 1 : 2), yield=20%, m.p.: 186–188°C. ¹H NMR (DMSO-*d*₆, 500 MHz, δ ppm): 1.18–1.51 (m, 6H), 2.38–2.42 (m, 4H), 2.67 (s, 3H), 3.34–3.45 (m, 1H, CH-N cyclohexyl), 7.20–7.26 (d, $J=8.4$ Hz, 1H), 7.64–7.66 (m, 5 H), 7.83–7.84 (d, $J=8.4$ Hz, 2H), 7.93–7.95 (d, $J=8.4$ Hz, 2H), 8.19 (s, 1H, CH=N), 8.20–8.26 (d, $J=8.4$ Hz, 1H), 8.60 (s, 1H). MS: m/z 538 (100%). Anal. Calcd. for C₃₀H₂₇ClN₆O₂ (538.19): C, 66.85; H, 5.05; Cl, 6.58; N, 15.59; found C, 66.73; H, 5.14, Cl, 6.55, N, 15.41.

General procedure for the preparation 21 and 22

A solution of 4-aminobenzoic acid **10** in DMF (10 ml) was added to benzene sulfonyl chloride or 2-nitrobenzene sulfonyl chloride (10 mmol) in DMF (10 ml), with the addition of a few drops of trimethylamine (TEA), and was stirred for 24 h at 70°C. The excess DMF was evaporated, and the formed solid washed with ether and recrystallized from ethanol.

4-(Phenylsulfonamido)benzoic acid (21)

White solid, m.p.: 276–278°C. IR (4000–400 ν /cm): 3272 (NH), 1677 (CO), 1332 (SO sym), 1163 (SO asym). ¹H NMR (DMSO-*d*₆, 500 MHz, δ ppm): 6.89.6.92 (d, 2H, $J=8.8$ Hz), 7.29–7.31(m, 1H), 7.42–7.44(m, 2H), 7.53–7.56 (d, 2H, $J=8.8$ Hz), 7.91–7.94 (m, 2H), 10.85 (s, 1H, NH D₂O exchangeable), 12.75 (s, 1H, COOH, D₂O exchangeable). MS: m/z 277 (M⁺, 100%). Anal. Calcd. for C₁₃H₁₁NO₄S (277.04): C, 56.31; H, 4.00; N, 5.05. Found: C 56.42; H, 4.01; N, 5.08.

4-((2-Nitrophenyl)sulfonamido)benzoic acid (22)

White solid, m.p. 282–285°C. IR (4000–400 ν /cm): 3213 (NH), 1697 (CO), 1336 (SO sym), 1162 (SO asym). ¹H NMR (ppm): 6.89.6.92 (d, 2H, $J=8.8$ Hz), 7.29–7.31 (m, 1H), 7.42–7.84–6.94–6.97 (d, 2H, $J=8.8$ Hz), 7.61–7.69 (m, 1H), 7.84–7.87 (d, 2H, $J=8.8$ Hz), 7.94–7.98 (m, 1H), 8.24–8.28 (m, 1H), 8.61–7.65 (m, 1H), 11.24 (s, 1H, NH, D₂O exchangeable), 11.471 (s, 1H, COOH, D₂O exchangeable). MS: m/z 322 (M⁺, 100%). Anal. Calcd. for C₁₃H₁₀N₂O₆S (322): C, 48.45; H, 3.13; N, 8.69; S, 9.95. Found: C, 48.49; H, 3.21; N, 8.62; S, 10.03.

General procedure for the preparation 24 and 25

To a solution of 3,4-diaminobenzoic (**23**) (10 mmol) in *o*-phosphoric acid (60 ml), compound **21** or **22** was added under dry conditions. The reaction mixture was gradually heated to 180°C, stirred for 4 h, allowed to cool to about 100°C, and poured in a large volume of rapidly stirred water. Ammonia solution was added until the solution was neutralized. The formed solid was collected, washed with water, and dried.

2-[4-(phenylsulfonamido)phenyl]-1H-benzo[d]imidazole-5-carboxylic acid (24)

Brown solid m.p. more than 300°C. $R_f=0.28$ (pet. ether/ethyl acetate, 1 : 1), yield=70%. ¹H NMR (DMSO-*d*₆) δ : 7.16–7.16 (d, 1H, $J=8.4$ Hz), 7.48–7.54 (m, 5Hs), 7.54–7.57 (d, 2H, $J=9.15$ Hz), 7.81–7.84 (d, 2H, $J=9.15$ Hz), 7.79–7.81 (d, 1H, $J=8.4$ Hz), 8.30 (s, 1H), 9.57 (s, 1H, NH, D₂O exchangeable), 12.02 (s, 1H, NH, D₂O exchangeable), 13.0 (s, 1H, OH, D₂O exchangeable). ¹³C NMR (DMSO-*d*₆, 500 MHz, δ ppm): 116.54, 120.15, 122.44, 127.05 131.33, 130.87, 135.67 (C=C aryl), 147.33 (=C-N), 151.98, (C=N), 168.58 (C=O). Anal. Calcd. for C₂₀H₁₅N₃O₄S (393.08) C, 61.06; H, 3.84; N, 10.68; S, 8.15. Found, C, 61.17; H, 3.77; N, 10.61; S, 8.27.

2-[4-(2-Nitrophenylsulfonamido)phenyl]-1H-benzo[d]imidazole-5-carboxylic acid (25)

Yellowish brown solid. m.p. more than 300°C. $R_f=0.3$ (pet. ether/ethyl acetate, 1 : 1), yield=66%. ¹H NMR

(DMSO-*d*₆) δ : 7.15–7.17 (d, 1H, $J=8.4$ Hz), 7.48–7.54 (m, 3H), 7.64–7.66 (d, 2H, $J=9.15$ Hz), 7.81–7.84 (m, 3Hs), 8.03–8.04 (d, 1H, $J=8.4$ Hz), 8.23 (s, 1H), 10.21 (s, 1H, NH, D₂O exchangeable), 12.55 (s, 1H, NH, D₂O exchangeable), 13.54 (s, OH, D₂O exchangeable). ¹³C NMR (DMSO-*d*₆, 500 MHz, δ ppm): 117.95, 122.85, 123.29, 129.461, 130.49, 131.21, 139.72 (C=C aryl), 148.26 (=C-N), 152.29, (C=N), 170.62 (C=O, carboxylic). Anal. Calcd. for C₂₀H₁₄N₄O₆S (438.06) C, 54.79; H, 3.22; N, 12.78; S, 7.31. Found, C, 54.77; H, 3.19; N, 12.75; S, 7.30.

2,3-Dioxo-1,2,3,4-tetrahydroquinoxaline-6-carboxylic acid (26)
Compound **26** [29] was prepared according to the previously described method by Khairat *et al.* [30].

2,3-dihydrazinylquinoxaline-6-carboxylic acid (27)

To compound **26** (10 mmol) was added hydrazine hydrate 98% (3 ml) and ethanol (20 ml). The reaction mixture was refluxed for 2 h left to cool and poured on water. The solid obtained was filtered, and washed with pet. ether. $R_f=0.4$ (chloroform/ethanol, 1 : 1), yield=70%, m.p.: more than 300°C. IR (KBr) $\nu_{\max}/\text{cm}^{-1}$: 3421 (NH and NH₂) 3336 (NH and NH₂), 1690 (C=O acidic), 1587 (C=N quinoxaline). ¹H NMR (DMSO-*d*₆, 500 MHz, δ ppm): δ 6.44 (br., 2H, D₂O exchangeable), 7.81–7.84 (d, $J=8.70$ Hz, 1H), 8.07–8.10 (d, $J=8.70$ Hz, 1H), 8.42 (s, 1H), 11.54 (s, 1H, OH, D₂O exchangeable). Anal. Calcd. for C₉H₁₀N₆O₂ (234.09): C, 46.15; H, 4.30; N, 35.88. Found C, 46.00; H, 4.27; N, 35.91.

General procedure for the preparation 28 and 29

A solution of compound **27** (10 mmol) dissolved in 15-ml ethanol was added to pyrazole derivative **4** or **5** (10 mmol), and then gl. acetic acid (2 ml) was added. The reaction was refluxed for 12 h. The excess solvent was allowed to evaporate, and then the precipitated product was crystallized from ethanol to achieve compounds **28** or **29**, respectively.

2-[(3-Methyl-1-phenyl-5-chloro-1H-pyrazol-4-yl)methylenehydrazinyl]-3-[(3-methyl-1-phenyl-5-chloro-1H-pyrazol-4-yl)methylenehydrazinyl]-quinoxaline-6-carboxylic acid (28)

$R_f=0.75$ (ethyl acetate/ pet. ether, 1 : 1), yield=55%, m.p. 252–255°C. ¹H NMR (DMSO-*d*₆, 500 MHz, δ ppm): δ 2.69 (s, 3H), δ 2.71 (s, 3H), 7.43–7.52 (m, 5H), 7.55–7.64 (m, 5H), 7.78 (s, 2H), 7.99–8.02 (d, 1H, $J=8.70$ Hz), 8.32–8.35 (d, 1H, $J=8.70$ Hz), 8.54 (br., 2H, D₂O exchangeable), 8.61 (s, 1H), 11.75 (s, 1H, OH, D₂O exchangeable). ¹³C NMR (DMSO-*d*₆, 125 MHz, δ ppm): 13.33, 123.03, 124.72, 125.15, 126.03, 127.22, 127.95, 129.6, 129.88, 130.43, 134.31,

136.57, 137.63, 139.65, 146.11, 149.65, 166.51. MS (m/z , %): 640 (M⁺, 62.0%), 638 (M⁺, 100%). Anal. Calcd. for C₃₁H₂₄C₁₂N₁₀O₂ (638.15): C, 58.22; H, 3.78; Cl, 11.09; N, 21.90. Found: C, 58.40; H, 3.82; Cl, 10.89; N, 21.77.

2-[(3-Methyl-1-phenyl-5-(piperazin-1-yl)-1H-pyrazol-4-yl)methylenehydrazinyl]-3-[(3-methyl-1-phenyl-5-(piperazin-1-yl)-1H-pyrazol-4-yl)methylenehydrazinyl]-quinoxaline-6-carboxylic acid (29)

$R_f=0.27$ (ethylacetate/petroleum ether, 3 : 1), yield=61%, m.p.: 300–303°C. IR (KBr) $\nu_{\max}/\text{cm}^{-1}$: 3500 (OH and NH hydrogen bonded centered at 3000 cm⁻¹), 1672 (C=O acidic), 1602 (C=N). ¹H NMR (DMSO-*d*₆, 500 MHz, δ ppm): 2.01(br., 2H, D₂O exchangeable), δ 2.68 (s, 6H), 3.13–3.15 (m, 8H), 3.29–3.39 (m, 8H), 7.44–7.56 (m, 10H), 7.60–7.63 (d, 1H, $J=8.70$ Hz), 7.76 (s, 2H), 8.41 (br., 2H, D₂O exchangeable), 8.27–8.30 (d, 1H, $J=8.70$ Hz), 8.62 (s, 1H), 11.72 (s, 1H, OH, D₂O exchangeable). ¹³C NMR (DMSO-*d*₆, 125 MHz, δ ppm): 13.03, 50.03, 52.93, 117.43, 121.13, 122.35, 126.85, 125.55, 126.79, 127.78, 129.18, 129.25, 130.31, 136.55, 137.43, 139.67, 140.20, 149.67, 151.65, 166.55.

MS: m/z 738(M⁺, 50%). Anal. Calcd. for C₃₉H₄₂N₁₄O₂ (738.36): C, 63.40; H, 5.73; N, 26.54. Found: C, 63.34; H, 5.82; N, 26.64.

Antiviral activity

Activity of the target compounds against bovine viral diarrhea virus based on plaque reduction assay

The plaque antiviral assay was done as described early by Whitby *et al.* [25] with some modifications. In brief, 4×10⁵ MDBK cells were cultured in 6-well culture plates and allowed to grow overnight. The cells were infected with BVDV at an multiplicity of infection of 0.1; the virus titer was 38×10⁴ PFU/ml. After 1.5 h of incubation, the virus was removed and replaced with 2 ml of complete Dulbecco's Modified Eagles Medium (containing 0.5% sea plaque agarose and different concentrations of tested compounds). After 3 days of incubation in 5% CO₂, 37°C incubator, the cells were fixed with 10% formaldehyde for 2 h at room temperature. The agarose layer was removed, and the fixed cells were stained with 0.3% methylene blue. Plaques were counted with naked eye in comparable to the positive control.

Antiviral activity of compounds 12 and 13 against hepatitis C virus infectious system

Huh7.5.1 (4×10⁴) cells were cultured in collagen precoated slides (Thermo Scientific (Massachusetts,

United States) Lab-Tek Chamber Slide) overnight. Cells were infected with HCV infectious system JFH1 [31] for 2 h. Then, JFH1 [31] was replaced with media containing different concentrations of compounds **12** and **13** in a dose-dependent manner. After 48 h, cells were fixed using 4% paraformaldehyde for 1 h, permeabilized with 0.1% Triton-X 100 for 8 min, followed by blocking with Blocking One Histo (Nacalai Tesque) for 1 h at room temperature. After staining with mouse anti-HCV core monoclonal antibody, 2H9 [31] as first antibody for overnight at 4°C and Alexa Fluor-555 goat anti-mouse IgG secondary antibody at 37°C for 2 h, the nuclei were finally stained using Invitrogen Prolong Diamond Antifade Mountant with DAPI. Wells were checked using a BZ-X 710 KEYENCE fluorescence microscope and analyzed using a BZ-X analyzer. Relative infectivity was obtained by normalization number of infected cells at different concentrations of each compound to number of infected cells at control wells (without compounds). IC50 values were measured with GraphPad Prism statistical program.

Viability assay:

Huh7.5.1 (4×10^4) cells were cultured in 96-well cell culture plate overnight. Cells were treated with different concentrations of compounds starting with 62.5–1000 µg/ml together with 10% of Invitrogen Alamar Blue viability reagent and left for 48 h CC₅₀ values were detected after reading optical density at 570 nm. DMSO was used as a control.

GOLD molecular docking study

The crystal structures of HCV polymerases in complex with its co-crystallized native ligand were retrieved from the Protein Data Bank, <http://www.rcsb.org/pdb/home/home.do> For each docking target, crucial amino acids of the active site were identified using data in PDB sum, <http://www.ebi.ac.uk/pdbsum/> These include: (a) for the active site, 'PDB: 2ijn' [32] was used with its native ligand: 221. The co-crystallized ligand coordinates are 8.816, 42.819, and 49.509, and using C366 (A) and S556 (A) as flexible residues. (b) For the allosteric site, 'PDB: 2hwh' [33] and 'PDB: 3frz' [34] were used with their bound ligands: RNA-960 and AG0577, and their ligand coordinates are 8.180, 33.87, and 73.33 and 42.699, 13.717, and 54.046, respectively, and using Y477(A), S476(A), and R501(A) as flexible residues in both of them. (c) For the thumb domain, 'PDB: 2wrm' [35] was used with its bound ligand: QQ3 and its coordinates are 40.060, 6.851, and 16.264, and W528(A), R422(A), and R501(A) were used as

flexible residues. (d) For the finger-loop site, 'PDB: 2wcx' [36] was used with its bound ligand: VGC and its coordinates are 29.31, 12.957, and 7.830, and R503(A) was used as a flexible residue. (e) For the NNI-I site, 'PDB: 2gir' [37] was used with its bound ligand: NN3 and its coordinates are -33.939, -18.827, and 33.384, and Y477(A) and S476(A) were used as flexible residues. (f) For the NNI-II site, 'PDB: 2giq' [37] was used with its bound ligand: NN2 and its coordinates are 9.09, -8.237, and -12.83 and Y448 (A) was used as a flexible residue.

The constructed 3D structures of the compounds investigated, namely, **12–17** and **29** were energetically minimized using MOPAC.

GOLD software package, version 5.2.2 (Cambridge Crystallographic Data Centre, Cambridge, UK), was used in this study [38]. The Hermes visualizer in the GOLD Suite was used to further prepare the receptors for docking. The region of interest used for GOLD docking was defined as all of the protein residues within the 10 Å of the reference ligands.

Default values of speed settings and all other parameters were used for both pose selection and enrichment studies. The structurally conserved water molecule was set 'on' with spin orientation enabled, and the set atom types function was 'on' for ligand and 'off' for the protein. The fitness function was set to the Gold Score fitness function with default input and annealing parameters. Hydrophobic fitting points were calculated to facilitate the correct starting orientation of the compound for docking by placing the hydrophobic atoms appropriately in the corresponding areas of the active site. The best docking poses were selected based on the gold fitness score and the critical interactions reported in the literature studies. GoldScore 'Allow early termination' and soft potentials were turned off, and 200% search efficiency was employed to allow maximal exploration of ligand conformation. When the top three solutions attained root mean square deviation (RMSD) values within 1.5 Å, docking was terminated. With respect to ligand flexibility, special care was taken by including options such as flipping of all planar RNR1R2, ring NH-R ring, and flip protonated carboxylic acids -(O=C)-OH, as well as torsion angle distribution and post-process rotatable bonds as default. The region of interest used for GOLD docking was defined as all of the protein residues within the 15 Å of the reference ligands. Default values of speed settings and all other parameters were used for both pose selection and enrichment

studies. The structurally conserved water molecule was set 'on' with spin orientation enabled, and the set atom types function was 'on' for ligand and 'off' for the protein. The fitness function was set to the GoldScore fitness function with default input and annealing parameters. Hydrophobic fitting points were calculated to facilitate the correct starting orientation of the compound for docking by placing the hydrophobic atoms appropriately in the corresponding areas of the active site. The best docking poses were selected based on the gold fitness score and the critical interactions reported in the literatures. We used 10 genetic algorithm docking runs with internal energy offset. For pose reproduction analysis, the radius of the binding pocket was set as the maximal atomic distance from the geometrical center of the ligand plus 3 Å. The top ranked docking pose was retained for the 3D cumulative success rate analysis. The genetic algorithm default settings were accepted as population size 100, selection pressure 1.1, number of operations 100 000, number of islands 5, niche size 2, migrate 10, mutate 95, and crossover 95. All other parameters accepted the default settings.

The selected flexible residues were set of free Rotamer Library Operation was set to 0° and 180°. Gold flexible ligand docking generated 10 poses of each ligand, which were ranked using the GoldScore scoring function. Default values were used for all other docking parameters. All of the compounds were energetically minimized using MOPAC with 100 iterations and minimum RMS gradient of 0.10. The top ranked pose with highest GoldScore fitness was analyzed using Accelrys Discovery studio to reveal the hydrogen bond interaction and binding mode within the binding domain.

Acute toxicity studies in experimental animals

The acute toxicity studies on the Wistar rats included in this study were approved ethically from the Medical Research Ethics Committee, National Research Centre, Cairo, Egypt under number 1449102021. Rats were maintained and studied according to local guidelines for animal care. Dulbecco's phosphate-buffered saline was used as the injected vehicle. Animals were divided into two groups, each group consists of 10 rats (120–140 g body weight, male Wistar rats). One group received orally a single dose of 0.375 mg/kg rat body weight of compound **12** and the other group was used as a control.

Identification of animals

Each cage was tagged having the description of study number, test substance code, dose, animal number,

cage number, date of initiation, and date of completion of the experiment. Lighting was controlled to give 12 h of artificial light (8 a.m. –8 p.m.) each day.

Husbandry

All animals were randomly selected and caged in a group of 10 in polypropylene cages fitted with wire mesh. The room temperature was maintained at 22±3°C.

Diet

Water and standard pelleted feed (animal house, National Research Center) were provided to the experimental animals.

Acclimatization

A minimum of 5 days of acclimatization was allowed before the commencement of the study.

Experimental design of acute toxicity studies

The acute toxicity study for treatment was performed using male rats. The animals were fasted overnight before the experiment and maintained under standard conditions. The visual observations of mortality, various changes in physical appearance, behavior (salivation, lethargy), and any injury or illness were conducted once daily.

Biochemical determinations

Assays including complete blood counts (hemoglobin, red blood cells count, white blood cells count, and platelets count), liver functions (aspartate transaminase, alanine transaminase [39], and albumin), and kidney functions (urea [40], and creatinine [41]) were assessed for all rats after 48 h and 15 days of injection using commercial kits (Bio-diagnostic).

Statistical analysis

The results were analyzed through one-way analysis of variance followed by Turkey's multiple comparison test. A value of *P* value less than 0.05 was considered statistically significant.

Killing and necropsy

All of the experimental animals were subjected to necropsy. Animals were killed by decapitation after ether anesthesia. All findings were recorded.

Histopathological investigation

For histopathological investigation, autopsy samples were taken from the liver and kidneys of rats in

different groups after 15 days of injection and fixed in 10% saline for 24 h. Washing was done in tap water and serial dilutions of alcohol (methyl, ethyl, and absolute ethyl). Specimens were cleared in xylene and embedded in paraffin at 56° in hot air oven for 24 h. Paraffin blocks were prepared for sectioning at 4- μ m thickness by a sledge microtome. The obtained tissue sections were collected on glass slides, deparaffinized, and stained by hematoxylin and eosin stain for examination through the light electric microscope [42].

Results and discussion

Rational design

The main objective of this investigation was the development of novel HCV antiviral agents through the design and synthesis of analogs to the lead compound JTK-109 (Fig. 2) by modifying its structure, trying to improve its properties, and evaluating the effect of structural changes, which were performed through the following:

- (1) Replacing the biphenyl system of the right-hand side of JTK-109 with hydrophobic moieties as benzenesulfonyl or substituted phenylpyrazolyl moieties in order to bind with the hydrophobic pocket of the allosteric binding site of the HCV NS5B polymerase enzyme. Moreover, the pyrazole rings carry polar groups capable of hydrogen bonding.
- (2) Introducing benzenesulfonyl or cyclohexyl moieties in position 1 of the benzimidazole ring capable of hydrophobic bindings.
- (3) Introduction of different linkers such as NH, which may act as H bonding donor, or N=CH, which may act as hydrophobic anchor.

- (4) Variation of substituents at the five position in the benzimidazole scaffold by H, or hydrophilic group as COOH, or H bond acceptor as NO₂.
- (5) Replacing the benzimidazole scaffold by the quinoxaline scaffold.

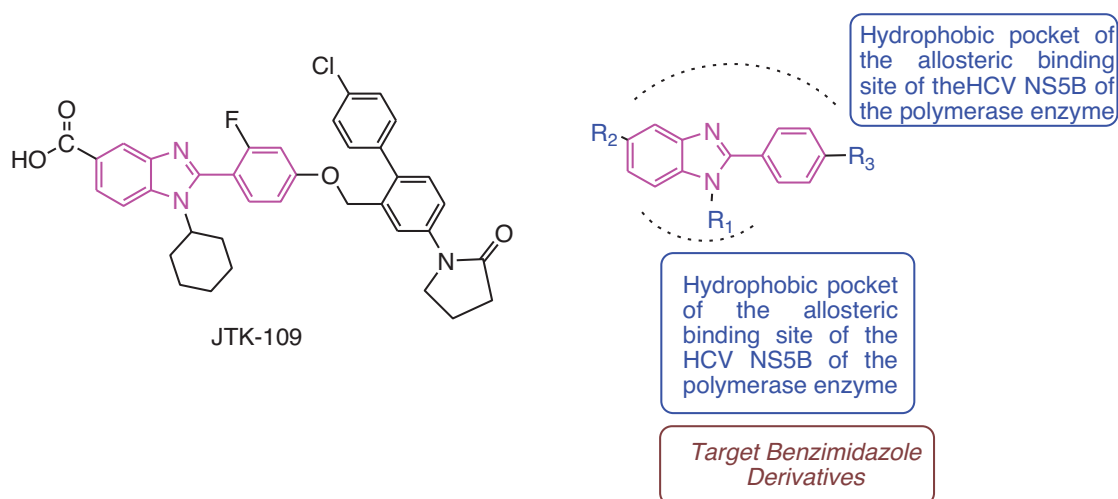
As illustrated in Fig. 2, our strategy was concerned about the preparation of the right-hand side of the target benzimidazole and quinoxaline derivatives. The right-hand side will involve the connection with benzenesulfonyl or pyrazole moieties (3-methyl-1-phenylpyrazol-4-carboxaldehyde; (Fig. 3), which possess various substituents at position 5 (Cl, piperidine, piperazine, substituted piperazine, and mercaptan) via condensation of the amino group with the aldehydic group attached to the pyrazole ring.

Chemistry

The first step, to ideally construct 'the right-hand side' of the target benzimidazole and quinoxaline derivatives containing pyrazole moiety, was to prepare the substituted piperazines **1-3** and the substituted 3-methyl-1-phenyl-pyrazoles **4-8** according to the reported procedures by Galal *et al.* [26,27,30] (Fig. 3). The pyrazoles **4-8** are considered as the right-hand side part used in the preparation of different Schiff bases by the condensation with the amino group of 2-(4-aminophenyl)-1*H*-benzimidazole derivatives or the quinoxaline derivatives representing the left-hand side was successfully performed to reach the target structures.

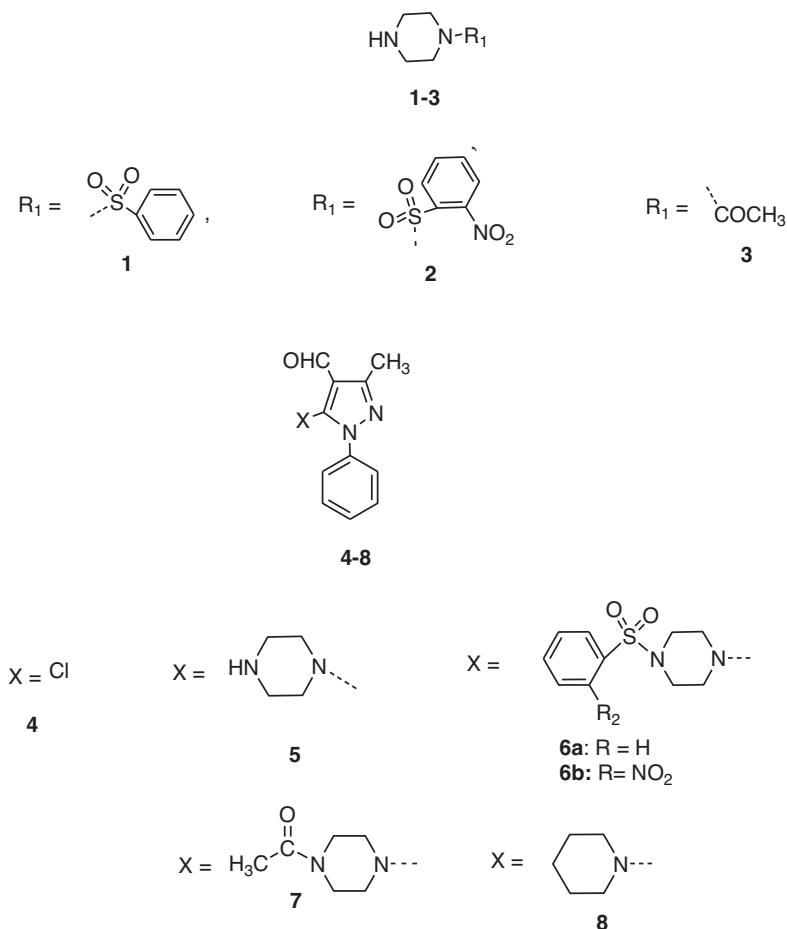
2-(4-Aminophenyl)-1*H*-benzimidazole (**9**) was prepared according to the described method by Galal *et al.* [26]. Stirring equimolar amount of **9** and

Figure 2



Strategy for the preparation of the target compounds.

Figure 3



Intermediates used in the synthesis of the target compounds.

benzenesulfonyl chloride or 2-nitro-benzene-1-sulfonyl chloride, respectively, in acetone and catalytic amount of triethyl amine gave the target mono-substituted benzenesulfonyl benzimidazole derivatives **10** and **11**, respectively (Scheme 14) [26]. Radiograph of single crystal of compound **10** was determined (Fig. 4) (c.f. supporting information). Refluxing one equivalent of **11** with two equivalents of both benzenesulfonyl chloride and sodium hydride in the presence of DMF as a solvent gave the target disubstituted benzenesulfonylbenzimidazole derivative **12** (Scheme 14). Similarly, refluxing **9** with two equivalents of both 2-nitro-benzene-1-sulfonyl chloride and sodium hydride in the presence of DMF gave the disubstituted 2-nitro-benzene-1-sulfonyl benzimidazole derivative **13** (Scheme 14). The target benzimidazole Schiff bases **14**, **15**, **16**, and **17** were prepared via condensation of **11** with the pyrazole derivatives **6a**, **6b**, **7**, or **8**, respectively (Scheme 14).

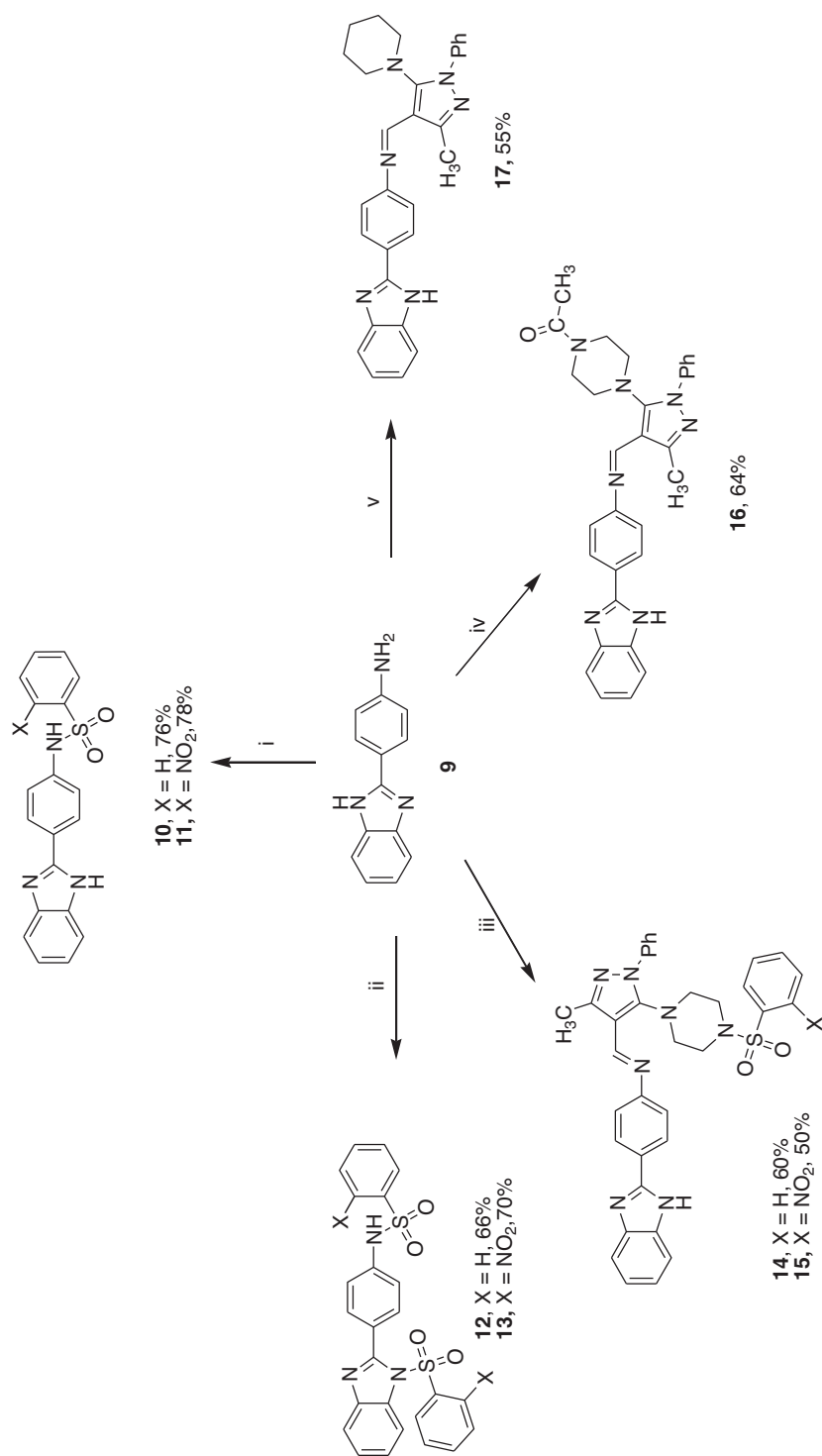
Reagent and conditions

(a) Benzenesulfonyl chloride, or 2-nitro-benzene-1-sulfonyl chloride, acetone, and catalytic amount of

triethyl amine; (b) benzenesulfonyl chloride, or 2-nitro-benzene-1-sulfonyl chloride, sodium hydride, dry DMF, reflux; (c) compound **6a** or compound **6b**, gl. acetic acid, reflux, and (d) compound **7**, gl. acetic acid, reflux 8 h v) **8**, gl. acetic acid,, reflux 8 h.

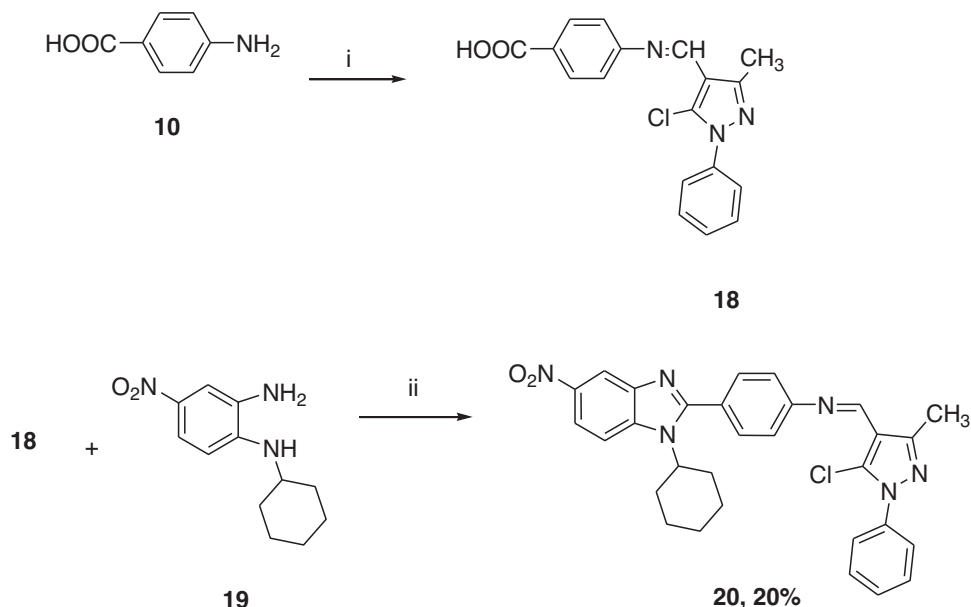
The formation of the Schiff base **18** via the condensation of 4-aminobenzoic acid **10** with compound **4**, in the presence of excess glacial acetic acid at 80°C, was achieved. The construction of the target benzimidazole derivatives with cyclohexyl group at position 1 was achieved via the formation of *N*₁-cyclohexyl-4-nitro-1,2-diamine **19** [28] and its cyclization with the Schiff base **18** to form the benzimidazole derivative **20**. Cyclization was performed by heating **18** and **19** in polyphosphoric acid (Scheme 15) to produce **20** in 20% yield. An attempt to perform dehydrohalogenation of the chloro group of **20** with different reagents as mercaptoacetic acid or different amines such as compounds **1-3** to form the target benzimidazole derivatives was unsuccessful and led to unidentified product.

Scheme 1



Synthesis of compounds 10–17.

Scheme 2



Synthesis of the target compounds 20.

Reagents and conditions

(a) Benzenesulfonyl chloride or 2-nitrobenzenesulfonyl chloride, DMF, few drops of TEA, stirring at 70°C and (b) 3,4-diaminobenzoic acid, *o*-phosphoric acid, 4 h.

The target compounds, benzenesulfonyl benzimidazole-5-carboxylic acid (**24**) and 2-nitrobenzenesulfonylbenzimidazole-5-carboxylic acid (**25**), were successfully synthesized starting from the condensation of 4-aminobenzoic acid (**10**) with benzenesulfonyl chloride (**21a**) and 2-nitrobenzenesulfonyl chloride (**21b**) in DMF and few drops of TEA to achieve the benzimidazoles **22** and **23**. Compounds **22** and **23** were reacted with 3,4-diaminobenzoic acid in *o*-phosphoric acid to obtain the desired target benzimidazole derivatives **24** and **25**, respectively (Scheme 16).

Reagents and conditions

(a) Benzenesulfonyl chloride or 2-nitrobenzenesulfonyl chloride, DMF, few drops of TEA, stirring at 70°C, (b) 3,4-diaminobenzoic acid, *o*-phosphoric acid, 4 h.

In addition, it was implemented to synthesize the promising quinoxaline derivatives. Quinoxaline-6-carboxylic acid **26** [29] was prepared according to the previously described method by Galal *et al.* [30], starting from cyclization of 1,2-phenylenediamine-4-carboxylic acid and oxalic acid. Treatment of **26** with hydrazine hydrate gave the quinoxaline dihydrazone derivative **27**, which was coupled with the pyrazole

aldehyde derivative **4** and **5** in ethanol and acetic acid to achieve the target quinoxaline derivatives **28** and compound **29**, respectively (Scheme 17).

Reagents and conditions

(a) Hydrazine hydrate 98%, ethanol, reflux, 2 h; (b) pyrazole **4**, ethanol, gl. acetic acid, reflux, 12 h; and (c) pyrazole **5**, ethanol, gl. acetic acid, reflux, 12 h.

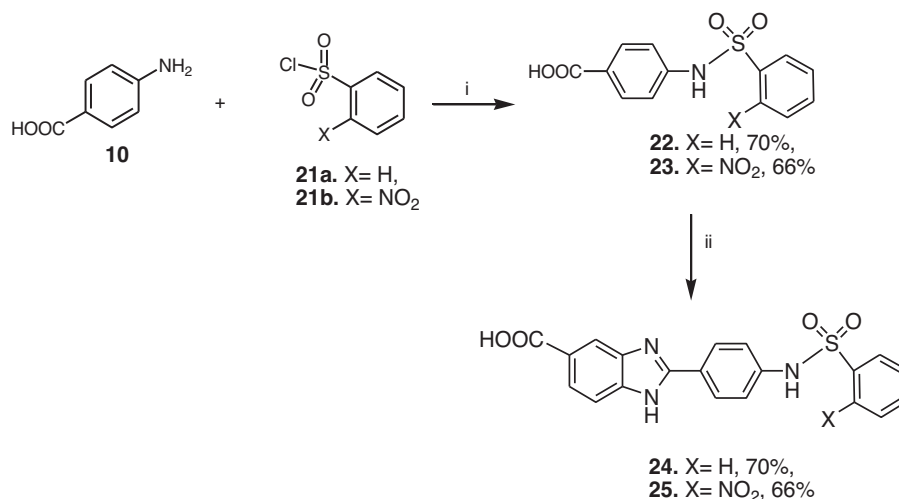
Antiviral activity of the target compounds against bovine viral diarrhea virus

Serial dilution of BVDV was used to infect MDBK cells, and the optimum range of viral concentration for testing of the target compounds was found to be 38×10^4 PFU/ml.

Assessment of anti-bovine viral diarrhea virus activity of the target compounds based on plaque assay

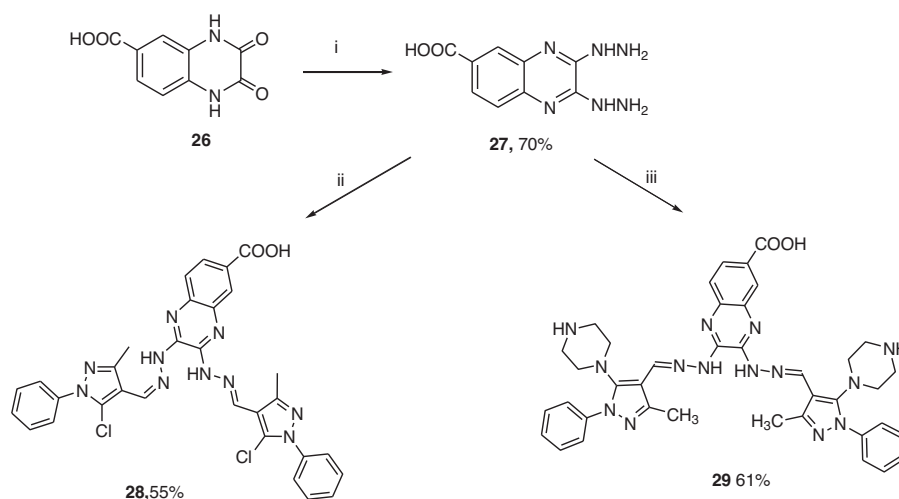
All of the tested compounds, **10–17**, **20**, **24**, **25**, **28**, and **29**, revealed competitive antiviral activities at a minimum concentration of 0.1 mg/ml, except compound **17** (Table 1). The order of activity at a minimum concentration of 0.01 mg/ml is **12=13>16>15>28>25>29>24=14=10>17>20>11**. All of the aforementioned compounds were toxic to MBDK cells at a higher concentration of 1.0 mg/ml, except for the two compounds **13** and **16**, which showed cell tolerability at 1.0 mg/ml. Compounds **12** and **13** displayed potent antiviral effects at a very low concentration of 0.01 and 0.1 mg/ml, respectively. On the contrary, compound **17** displayed cellular toxicity at 1.0 mg/ml and no antiviral activity at 0.1

Scheme 3



Synthesis of the target compounds **24** and **25**.

Scheme 4



Synthesis of compounds **28** and **29**.

and 0.01 mg/ml concentrations. In conclusion, compounds **12** and **13** showed a favorable profile at concentration of 0.01 mg/ml and potent antiviral activity without showing any cytotoxic effect.

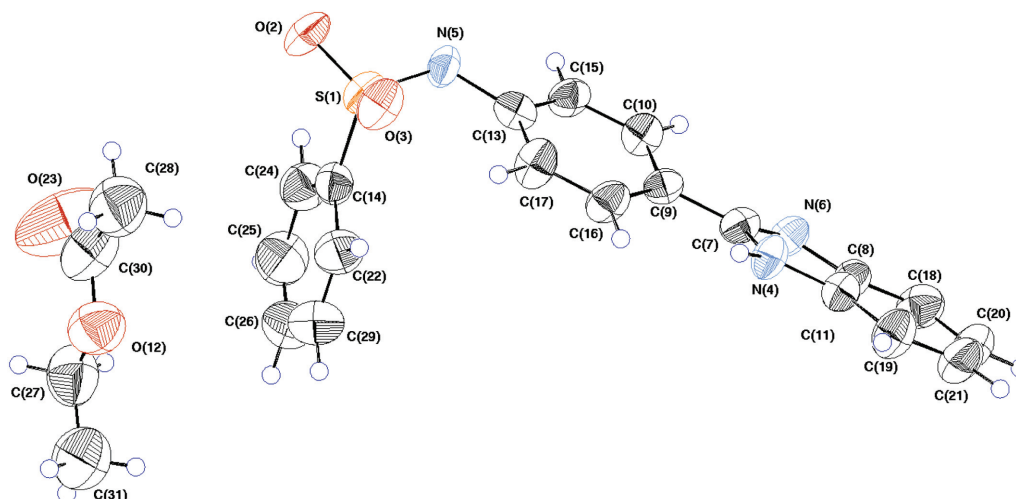
Testing anti-hepatitis C virus activity and cell viability of compounds **12** and **13**

Since the results of the antiviral plaque assay showed that compounds **12** and **13** were the most effective ones, so we proceeded to investigate the ability of these two compounds against HCV. The 50% inhibitory concentrations (IC₅₀) of compounds **12** and **13** were measured using a dose-dependent assay. Huh7.5.1 cells were infected with HCV, JFH1 [31] for 2 h. After that,

cells were treated with different concentrations of compounds **12** and **13** from 3 to 100 µg/ml for 48 h cells fixed with 4% paraformaldehyde and stained with anti-HCV core monoclonal Ab. After staining the nuclei with DAPI, BZ-X 710 KEYENCE fluorescence microscope was used to quantify the infected cells. Number of infected cells at each concentration of each compound was normalized with number of infected cells of control wells (without compounds). Both compounds showed a gradual decrease in infectivity. Compound **12** showed a complete inhibition at concentrations from 50 to 100 µg/ml and 98% inhibition at concentration of 25 µg/ml where compound **13** showed 100% complete

Table 1. Assessment of antiviral activity of the designed compounds based on plaque assay

Compd.	Conc.1 (1 mg/ml)	Conc.2 (0.1 mg/ml)	Conc.3 (0.01 mg/ml)
10	Death of cells	Negative	35×10^4 PFU/ml
11	Death of cells	Negative	39×10^4 PFU/ml
12	Death of cells	Negative	Negative
13	Negative	Negative	Negative
14	Death of cells	Negative	35×10^4 PFU/ml
15	Death of cells	Negative	11.5×10^4 PFU/ml
16	Negative	Negative	9×10^4 PFU/ml
17	Death of cells	23.5×10^4 PFU/ml	37.5×10^4 PFU/ml
20	Death of cells	Negative	38×10^4 PFU/ml
24	Death of cells	Negative	35×10^4 PFU/ml
25	Death of cells	Negative	27×10^4 PFU/ml
28	Death of cells	Negative	25×10^4 PFU/ml
29	Death of cells	Negative	29×10^4 PFU/ml
Positive control	38×10^4 PFU/ml		

Figure 4Radiograph of single crystal of compound **10** with one molecule of ethyl acetate.

inhibition only at concentration of $100 \mu\text{g/ml}$ (Fig. 5). IC_{50} values were calculated with nonlinear regression, $\log(\text{inhibitor})$ versus normalized response. The IC_{50} values were $9.358 \mu\text{g/ml}$ ($19.1 \mu\text{M}$) and $28.58 \mu\text{g/ml}$ ($49.4 \mu\text{M}$) for compounds **12** and **13**, respectively.

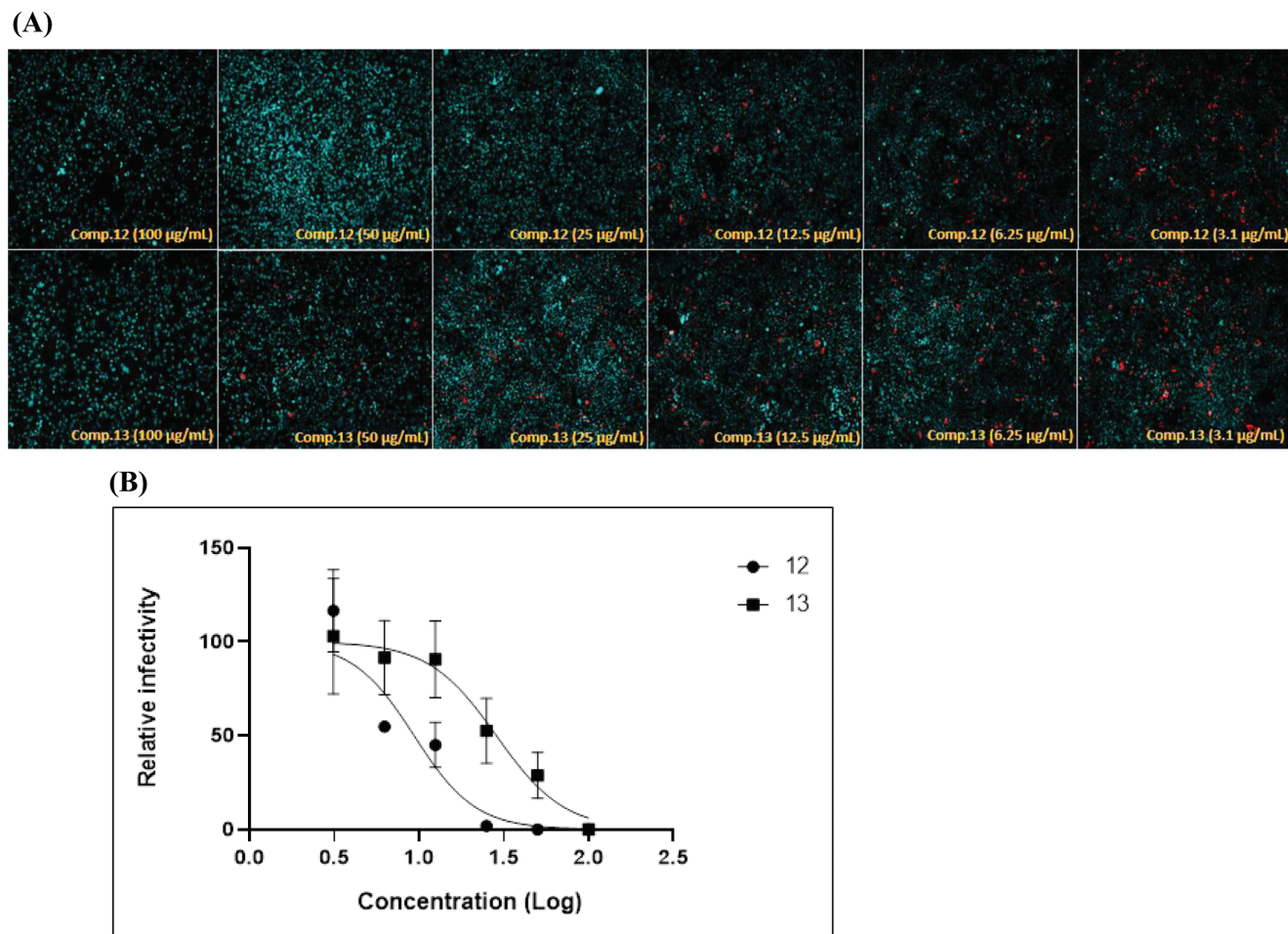
Moreover, cell viability was measured using Invitrogen Alamar Blue viability reagent for compounds after treating the Huh 7.5.1 cells with different concentrations of compounds from 62.5 to $1000 \mu\text{g/ml}$ together with 10% of Invitrogen Alamar Blue viability reagent for 48 h. The DMSO was used as a control (Fig. 6). The 50% cytotoxic concentration (CC_{50}) values were $367.885 \mu\text{g/ml}$ ($752.2 \mu\text{M}$) and $858.325 \mu\text{g/ml}$ ($1480 \mu\text{M}$) for compounds **12** and **13**, respectively.

According to the values of IC_{50} and CC_{50} , the selective index of tested compounds was calculated which was 39.3 for compound **12** and 30.03 for compound **13**, which means that compound **12** is the most promising compound.

Molecular docking

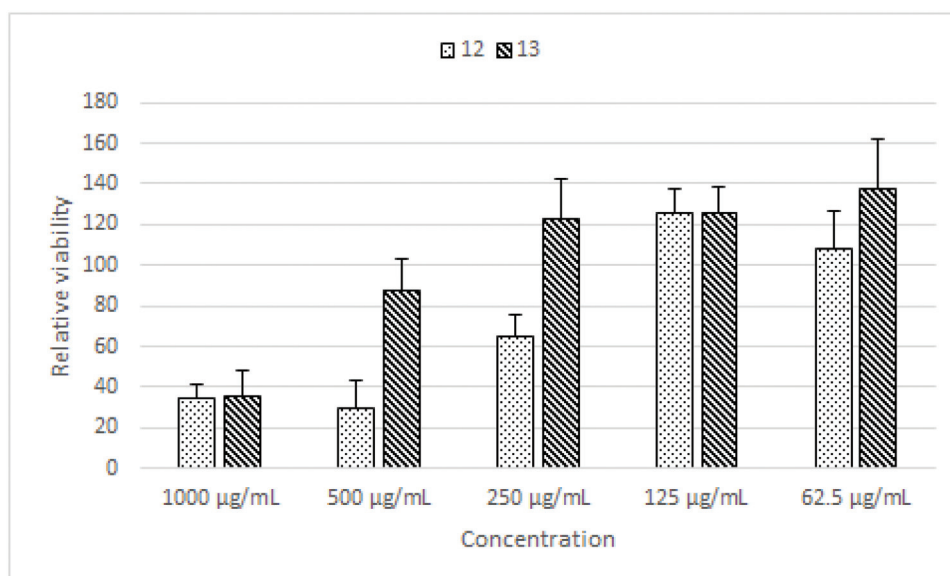
The compounds **12–17** and **29** which revealed the best binding affinity into HCV-NS5B RNA polymerases were initially subjected to screening into all the potential binding domains of six different polymerases (PDB: 2ijn [32], 2hwh [33], 2wrn [35], 2wcx [36], 2gir [37], and 2giq [37]). These sites included the active, allosteric, thumb domain, Finger-loop, NNI-I, and NNI-IV sites, respectively, as shown in Table 2.

Figure 5



(a, b) Antiviral activities against HCV infectious system: Huh7.5.1 cells were cultured for overnight. Then cells were challenged with JFH1 for 2 h. After that, the cells were treated with compounds **12** and **13** in a dose-dependent method for 48 h. Cells were fixed with paraformaldehyde and immunofluorescence procedures were accomplished. (a) Number of infected cells (red color) at different concentration of compounds were normalized to number of infected cells of control (without compounds) to calculate the 50% inhibitory concentration (IC_{50}). (b) Results were expressed as mean \pm SD. HCV, hepatitis C virus.

Figure 6



For cell viability, Huh7.5.1 cells were cultured for overnight. Cells were treated with compounds **12** and **13** at different concentrations plus 10% Alamar Blue viability reagent. After 48 h, optical density at 570 nm was measured and CC_{50} values were calculated. Results are expressed as mean \pm SD.

Table 2. The docking results for the best candidates (12–17, 29) into six different hepatitis C virus-NS5B RNA polymerases in comparison to their native bound inhibitors according to GOLD5.2.2 program

Site (PDB)	Compd.	GoldScore	Site (PDB)	Compd.	GoldScore	Site (PDB)	Compd.	GoldScore
Active site (PDB: 2ijn)	12	64.98	Allosteric site (PDB: 2hwh)	12	82.38	Thumb domain site (PDB: 2wrm)	12	75.49
	13	77.44		13	79.92		13	74.53
	14	65.65		14	71.96		14	85.41
	15	85.26		15	71.12		15	80.84
	16	63.10		16	78.12		16	83.05
	17	66.13		17	56.83		17	77.23
	29	98.82		29	74.32		29	86.37
	221a	58.34		RNA-960b	69.04		QQ3c	68.16
Finger loop site (PDB: 2wcx)	12	57.21	NNI-1 site (PDB: 2gir)	12	75.00	NNI-2 site (PDB: 2giq)	12	70.03
	13	64.97		13	64.66		13	74.63
	14	62.86		14	78.87		14	71.49
	15	56.13		15	84.09		15	75.97
	16	50.39		16	64.22		16	71.08
	17	59.72		17	59.34		17	63.22
	29	73.43		29	83.29		29	84.282
	VGCd	50.82		NN3e	64.93		NN2f	69.77

^a(2 R,3 R)-3-[[3,5-Bis(trifluoromethyl)phenyl]amino]-2-cyano-3-thioxopropanamide.

^b4-Methyl-n-((5e)-5-[(5-methyl-2-furyl)methylene]-4-oxo-4,5-dihydro-1,3-thiazol-2-yl)benzenesulfonamide.

^c(3 R)-3-(4-Methyl-1,3-dioxo-1,3-dihydro-2H-pyrrolo[3,4-c]quinolin-2-yl)hexanoic acid.

^d6-Cyclohexyl-4-methyl-5-phenyl-4H-thieno[3,2-b]pyrrole-2-carboxylic acid.

^e3-[[isopropyl[(trans-4-methylcyclohexyl)carbonyl]amino]-5-phenylthiophene-2-carboxylic acid.

^f1-(2-Cyclopropylethyl)-3-(1,1-dioxido-2H-1,2,4-benzothiadiazin-3-yl)-6-fluoro-4-hydroxyquinolin-2(1H)-one.

Interestingly, the most active derivatives **13**, **16**, and **12** revealed selective binding affinities to the allosteric site with GoldScores of 79.92, 78.12, and 82.38, respectively, as shown in Table 2. However, compound **29** exhibited nonselective binding affinities, which was confirmed by its highest GoldScores of 98.82, 74.32, 86.37, 73.43, 83.29, and 84.28 into almost all of the binding sites.

These initial docking results are matched with our assumption and rational design that these derivatives act as allosteric inhibitors by blocking polymerase activity before the polymerization process.

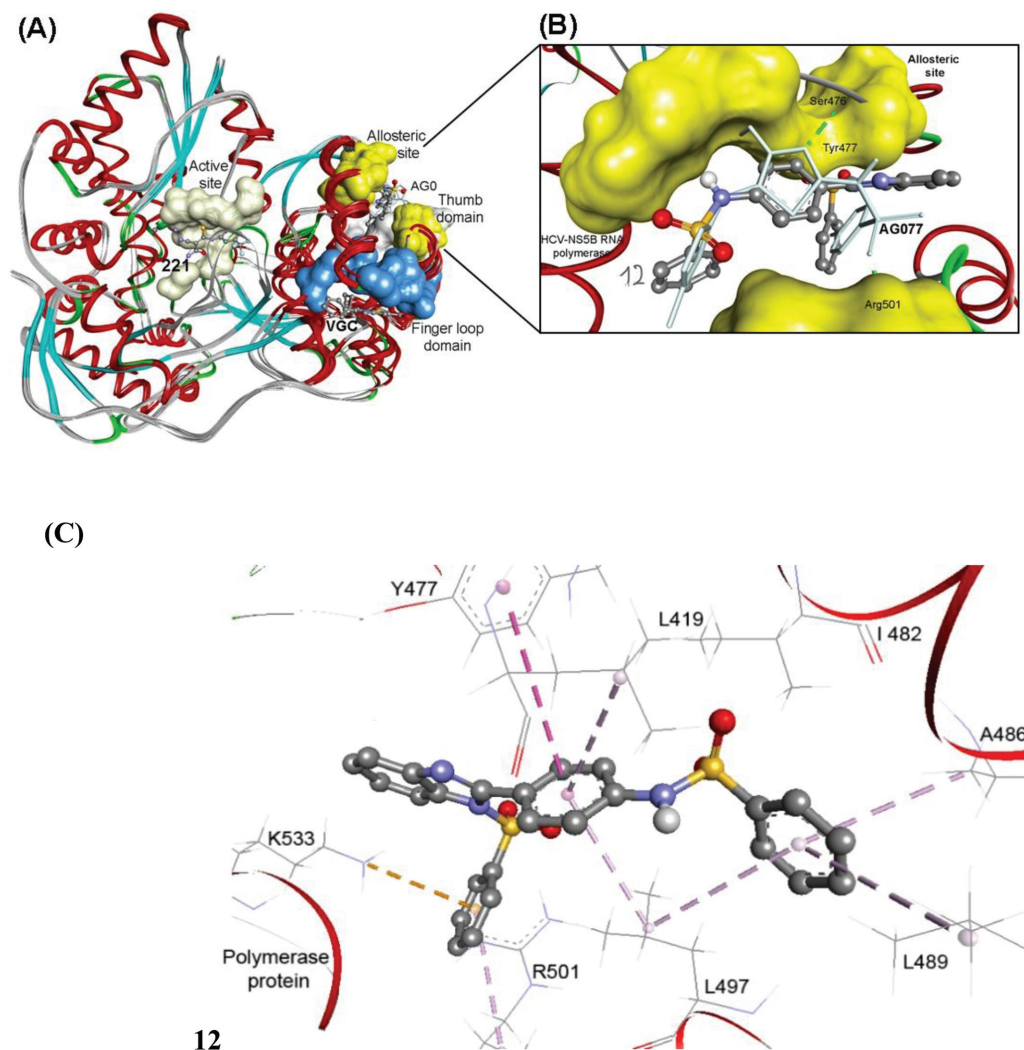
Interestingly, the most active compound **12** exhibited the best binding into the allosteric site with the smallest RMSD of 1.70 Å and one hydrogen bond with the key amino acid Y477 as shown in Fig. 7b. In contrast, compound **12** revealed poor binding affinities of 64.98 and 57.21 GoldScore into the active site and the finger-loop site of polymerase targets, respectively.

On docking of compound **12**, it revealed low GoldScore fitness of 70.43. Compound **12** binds into the polymerase enzyme by many hydrophobic interactions as illustrated in Fig. 7c. Its 2-phenyl ring interacts hydrophobically with Y477, L419, and

L497. It binds hydrophobically through its two side chain phenyl rings with A486, L489, L497, R501, and K533. The 2-anilino ring interacts by hydrophobic and π - π interactions with L419, L497, and Y477. The terminal phenyl ring interacts hydrophobically with A486, L489, and L497.

Moreover, the amino acid residues involved in the aforementioned binding modes of these compounds suggest that they act exclusively targeting the allosteric sites of the HCV-NS5B RNA polymerases. Furthermore, the crystal structures of the hepatitis-C virus polymerase enzyme (pdb: 3FRZ) [34] in complex with its co-crystallized native ligand: (AG0577): (6 R)-6-Cyclopentyl-6-[2-(2,6-diethylpyridin-4-yl)ethyl]-3-[(5,7-dimethyl [1,2,4] triazolo[1,5-*a*] pyrimidin-2-yl)methyl]-4-hydroxy-5,6-dihydro-2H-pyran-2-one, were used as an additional HCV-NS5B RNA polymerase enzyme for the detailed study on the allosteric site. It has an overall quality at a glance of 91% for chain A. The crucial amino acids of the active site were identified using data in PDB sum, <http://www.ebi.ac.uk/pdbsum/> These key amino acids are L419, R422, M423, H475, S476, I482, R501, and W528. The constructed 3D structures of the synthesized compounds, **12–17**, **20** were energetically minimized using MOPAC package.

Figure 7



(a) The molecular overlay view of HCV-NS5B RNA polymerases active site (PDB: 2ijn)¹, allosteric site (PDB: 2hwh), thumb domain site (PDB: 2wrm), finger-loop site (PDB: 2wcx), NNI-I site (PDB: 2gir), and NNI-II site (PDB: 2giq) showing the binding site in different colored surface views. (b) The binding mode of compound **12** into the allosteric site of HCV NS5B polymerase (PDB code: 2hwh), in which its benzimidazole ring was oriented into hydrophobic pocket region and protrude out the allosteric site exhibiting one hydrogen bond with Tyr477 amino acid. (c) Binding mode of interaction of compound **12** into polymerase enzyme (pdb code: 3FRZ). It interacts into the polymerase enzyme by many hydrophobic interactions through its 2-phenyl ring and its two side chain phenyl rings with and L419, Y477, A486, L489, L497, R501, and K533. HCV, hepatitis C virus.

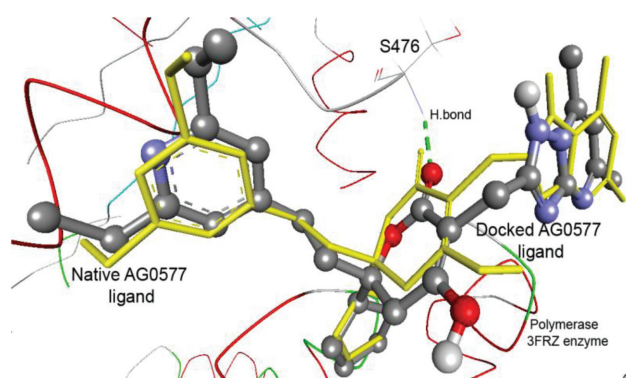
GOLD software package, version 5.2.2 (Cambridge Crystallographic Data Centre) [38], was used in this study. The Hermes visualizer in the GOLD Suite was used to further prepare the receptors for docking. The top ranked pose with highest GoldScore fitness was analyzed using Accelrys Discovery studio to reveal the hydrogen bond interaction and binding mode within the binding domain. The accuracy of docking by GOLD 5.2.2. software program was initially validated and confirmed by re-docking of co-crystallized (AG0577) ligand into the binding domain of the polymerase enzyme (pdb: 3FRZ) [34]. As shown in Fig. 8, the docked pose was closely aligned onto the native bound position within RMSD of 0.12 Å as shown in Fig. 8 and Table 3. This result denoted the high accuracy and

successful application of the GOLD program utilizing the polymerase 3D structure (pdb: 3FRZ), thus enable further docking study for the synthesized compounds. The GOLD molecular docking study of the assigned compounds revealed that they were docked within GoldScore fitnesses of 69.78–80.71. Substantially, these compounds bound by up to three hydrogen bonds between their sulfoxide moieties (S=O) and/or heteroaromatic pyrazole (C=N) groups and the amino acids R422 (NH) and S476 (NH). The compounds were docked within RMSD from the co-crystallized ligand of 0.86–3.86 Å.

The docking mode of compound **15** into polymerase enzyme is shown in Fig. 9. It exhibits a high GoldScore fitness of 80.41, and it provides two hydrogen bonds'

interaction between the pyrazole C=N and the R422 backbone NH in the HCV polymerase protein. Moreover, it provides key hydrophobic interactions between its benzimidazole ring and I482, A486, and L497 amino acids. The 2-phenyl ring occupied two small hydrophobic pockets formed by adjacent amino acid residues, including L419, M423, and L497. However, the terminal pyrazole-2-phenyl moiety exhibits an electrostatic attraction and hydrophobic interaction with K533 amino acid. Further observation of compound **15** displayed an unfavorable clash interaction of *o*-nitrophenyl-sulfonyl fragment with R501 amino acid.

Figure 8



Validation of the accuracy of GOLD docking by docking of the native AG0577 ligand into polymerase (pdb code: 3FRZ). The docking ligand (balls and sticks) seems identically superimposed onto the native co-crystallized one (yellow sticks) within RMSD of 0.12 Å. RMSD, root mean square deviation.

Structure activity relationship

Regarding the *in vitro* anti-BVDV activity, some relations were concluded linking structure to activity. All of the tested compounds were found to possess high antiviral activity at minimum concentration 0.1 mg/ml except compound **17**, which was the least active compound at concentrations 0.1 mg/ml (23.5×10^4 PFU/ml) and 0.01 mg/ml (37.5×10^4 PFU/ml). Consequently, the structure-activity relationship was deduced by comparing the activity of the compounds measured at minimum concentration 0.01 mg/ml. Compounds **12** and **13** showed the most potent activity, among the tested compounds, regarding the two tested concentrations of 0.1 and 0.01 mg/ml. Compounds **12** and **13** have in common two SO₂Ph moieties linked to the N atom in position 1 of the benzimidazole ring as well as to the NH of the anilino group. The nitro group present at the phenyl ring of the SO₂-phenyl group does not seem to influence the activity as both are highly potent.

Removing the SO₂-phenyl group from position 1 in the benzimidazolyl moiety for compounds **10** and **11**, and keeping it as substituent on the anilino moiety, showed its high effect on potency, as the activity decreases dramatically to be for **10** and **11** 35×10^4 and 39×10^4 PFU/ml, respectively. The SO₂Ph moiety present as a substituent at position 1 had a vital role in activity owing to the possible interactions of the π - π electrons of the phenyl ring, the possible hydrogen bonds that the SO₂ group could make in addition to favorable steric factors. Moreover, the presence of the polar nitro group on the phenyl ring

Table 3. GOLD docking results of 12–17 and 29 compounds into the polymerase enzyme (pdb: 3FRZ)

Compd.	GoldScore ^a				Hydrogen bonds			RMSD ^b (Å)
	Fitness	Internal vdw	External vdw	External HB	Atom of compd	Amino acid		
15	80.41	2.32	63.45	1.77	Pyrazole C=N	¹ HN of R422	2.25	
13	69.78	6.00	45.73	8.65	Pyrazole C=N	² HN of R422	3.42	
14	80.71	2.55	60.96	1.90	S=O	HN of K533	0.86	
29	71.09	-5.86	53.27	3.24	S=O	HN of S476		
					S=O	HN of Y477		
16	65.13	-2.98	48.19	1.87	Piperazine	O=C of W528	2.61	
17	70.89	-3.46	54.28	3.24	NH	HN of R422	2.86	
12	70.43	3.73	55.18	1.62	C=O	HN of R501	3.86	
AG0577^d	71.08	-6.48	53.15	0.72	COOH	O=C of F472	2.64	
					Me-C=O	HN of S476	0.12	

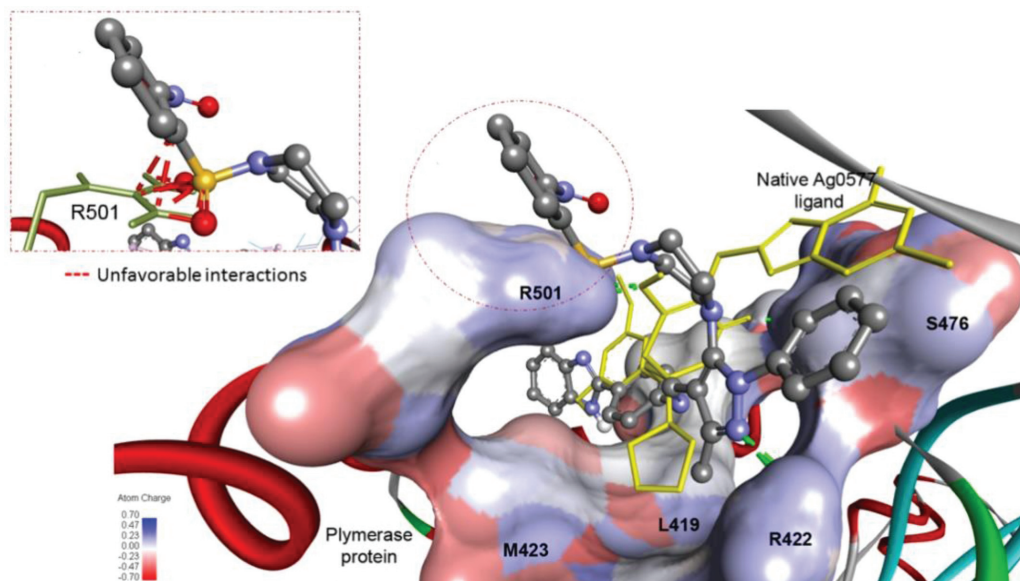
^aGoldScores have no unit and reflect fitness of the ligands. Higher values indicate higher affinities of the ligands to the protein

^bRoot mean square deviation.

^cNo hydrogen bond was detected.

^d(6 R)-6-Cyclopentyl-6-[2-(2,6-diethylpyridin-4-yl)ethyl]-3-[(5,7-dimethyl[1,2,4]triazolo[1,5-a]pyrimidin-2-yl)methyl]-4-hydroxy-5,6-dihydro-2H-pyran-2-one.

Figure 9



Docking of compound **15** into polymerase enzyme (pdb code: 3FRZ). Compound **15** is represented in ball and sticks. The nitrogen atom of pyrazole ring in compound **15** exhibited one hydrogen bond interaction with the amino acid residue R422, and the hydrogen bond is showed as green dashed line. Moreover, compound **15** is involved with some hydrophobic and electrostatic interactions, similar to the native ligand (AG0577), with the hydrophobic pockets formed by amino acid residues including L419, M423, L482, and L497.

of the SO₂-phenyl of compound **11** had a negative influence on activity as **11** is less potent than **10**. On the contrary, the nitro group has a positive influence on activity when it is present as a substituent on the SO₂Ph of compound **15**, as it was found to be more potent (11.5×10^4 PFU/ml) than **14** (35×10^4 PFU/ml) and compound **25** was more active (27×10^4 PFU/ml) than compound **24** (35×10^4 PFU/ml). Moreover, substitution at the 5-position of the benzimidazolyl moiety by the ionic carboxylic group favors the activity, as compound **25** (27×10^4 PFU/ml) was more active than **11** (39×10^4 PFU/ml). On the contrary, incorporating the nitro group at position 5 of the benzimidazolyl moiety of compound **20** (38×10^4 PFU/ml) does not have a positive effect on activity when position 1 is substituted by the hydrophobic cyclohexyl group as well as the presence of the =CH-pyrazolyl substituent at the anilino group.

Replacing the SO₂Ph moiety at the anilino N by =CH-pyrazole derivatives may increase the activity as compounds **16** (9×10^4 PFU/ml) and **15** (11.5×10^4 PFU/ml) are more active than **10** (35×10^4 PFU/ml) and **11** (39×10^4 PFU/ml) (c.f. Table 1). Compound **16** is more active than **15** and **14** which could be attributed to the presence of the favored acetyl group linked to piperazine ring in compound **16**. Substitution at position 4 of the pyrazolyl ring by a piperidyl group destroys the activity as compound **17** was the least active one among the tested series as mentioned before.

Regarding the quinoxaline derivatives, compound **28** carrying Cl as substituent on the pyrazolyl ring was more active than compound **29** having piperazine on the same ring.

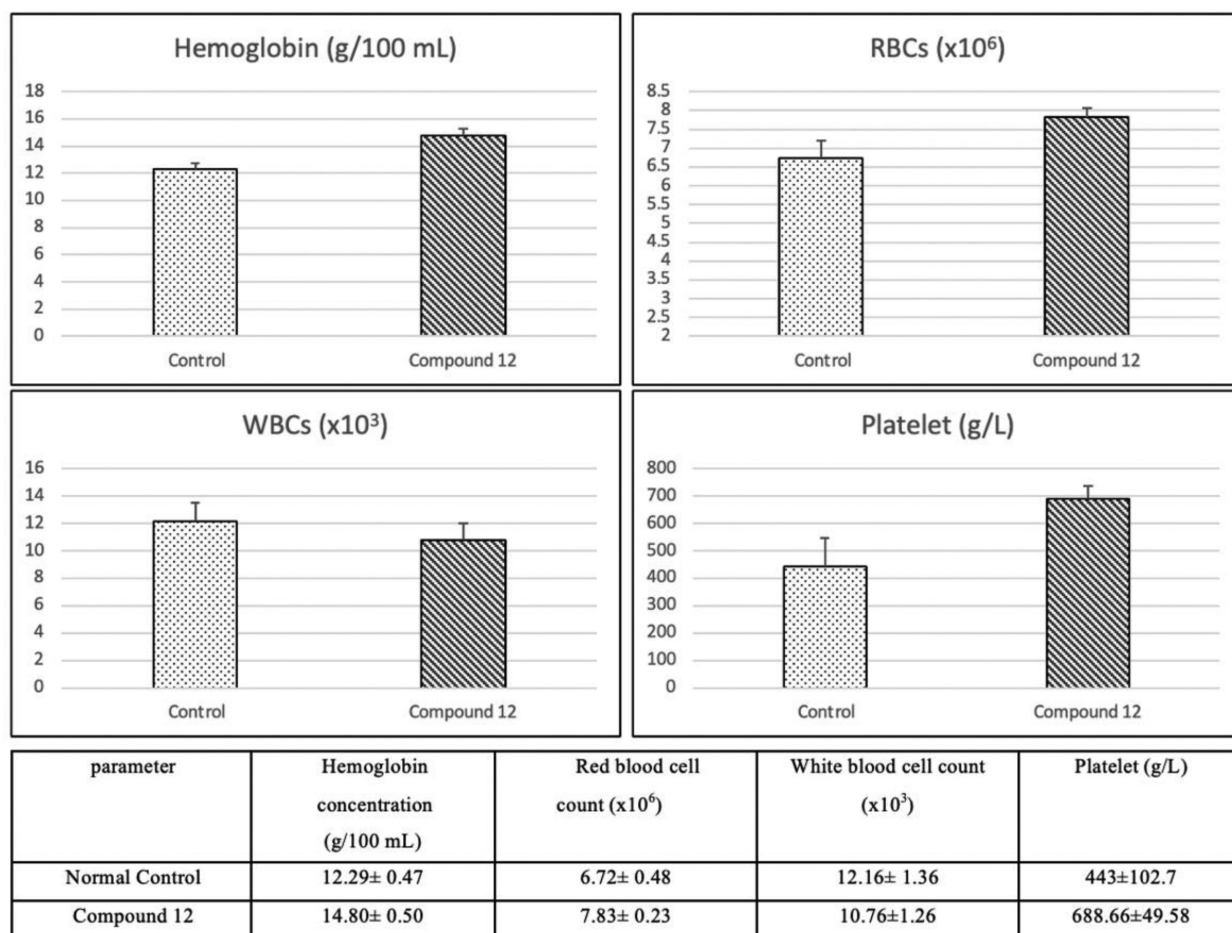
Acute toxicity studies in experimental animals

According to the results of antiviral activity, we concluded that compound **12** was the best to be proceeded in acute toxicity experiments. Compound **12** was administered orally to rats in a single dose of 0.375 mg/kg, which was calculated according to the effective dose in antiviral experiments. The data are expressed as the mean \pm SEM. The difference among the means has been analyzed by one-way analysis of variance followed by Turkey's multiple comparison test, a value of *P* value less than 0.05 was considered statistically significant.

All animals survived and appeared active and healthy throughout the study. The tested dose showed no toxic symptoms and mortalities for any of the tested animals, and did not affect the complete blood count including hemoglobin, red blood cell count as well as white blood cell counts. Although there was a slight increase in platelet count but it was insignificant (Fig. 10).

Biochemical parameters of liver were unchanged in comparison with controls except for aspartate transaminase, which showed insignificant modest increase (Fig. 11).

Figure 10



Effects of treatment with compound **12** on complete blood count (hemoglobin, red blood cell count, white blood cell count, and platelets). Results are expressed as mean±SEM of six rats.

Regarding kidney parameters, treatment with compound **12** displayed little decrease after 15 days of injections but it was still in the safe margins, with *P* value more than 0.05 (Fig. 12).

Histopathology

Concerning the histopathological observations, no gross abnormalities were noted for the animals when necropsied after 15 days (Fig. 13a and b). Liver showed healthy hepatic parenchyma in comparison with control (Fig. 13c). Kidneys showed slight histological changes including atrophied glomerular tuft with degenerated renal tubules (Fig. 13d).

Conclusion

Here, we report the investigation of the anti-BVDV efficacy of 12 benzimidazole derivatives and one quinoxaline derivative, ending up with 12 potent and one moderate anti-BVDV compounds. Anti-BVDV testings were used in our present study as surrogate for

disinfectant efficacy testing against human HCV. The most potent anti-BVDV compounds **12** and **13** were investigated for the anti-HCV activity and cell viability. The IC₅₀ values of **12** and **13** were found to be 19.1 and 49.4 μM respectively; their CC₅₀ were 752.25 and 1480 μM, respectively; and their SI were calculated to be 39.3 for **12** and 30.03 for **13**. The acute toxicity of compound **12** on rats was tested. No signs of toxicity, no deaths, and no significant changes were observed in the biochemical parameters of liver and kidneys.

Financial support and sponsorship

Nil.

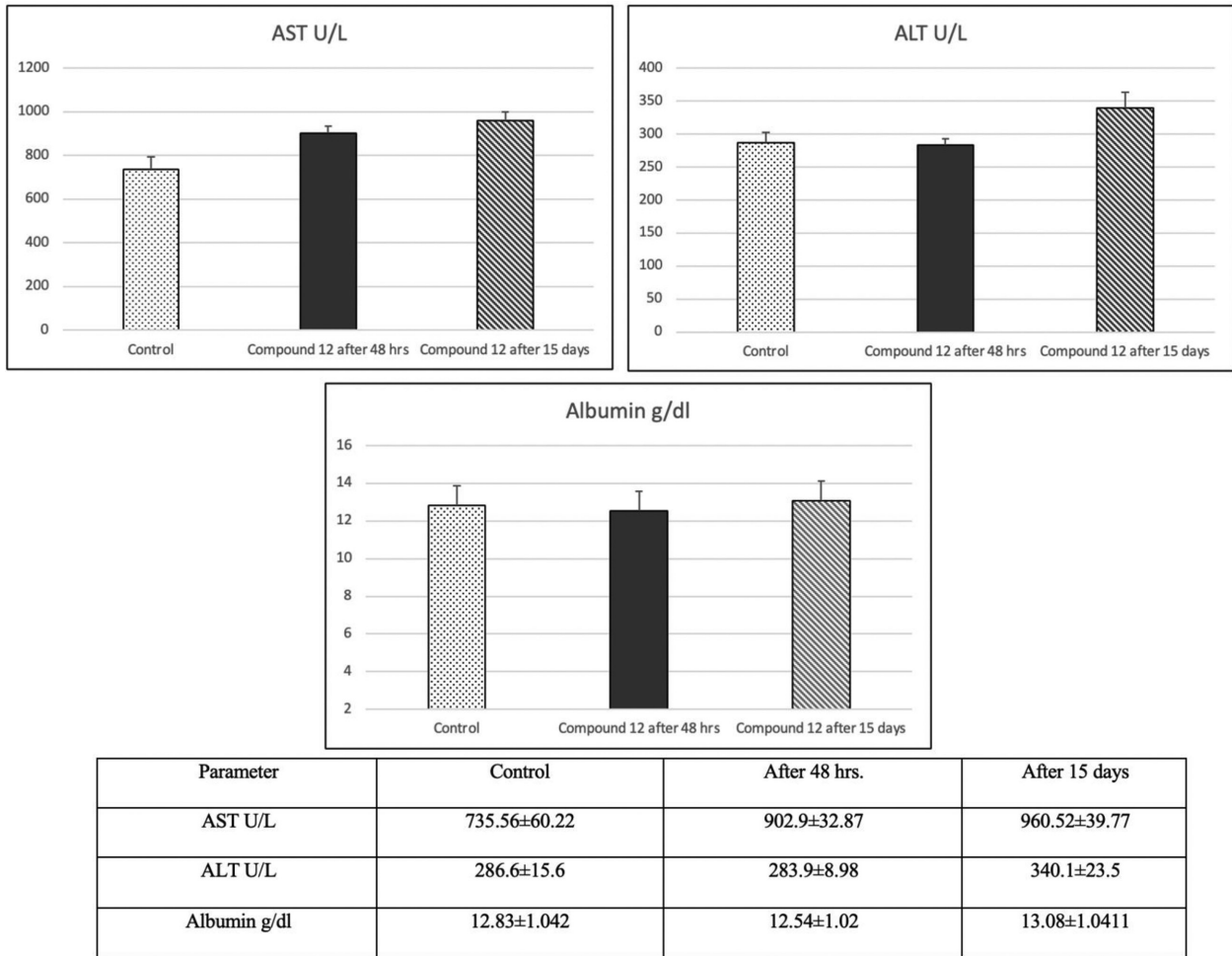
Conflicts of interest

There are no conflicts of interests.

Acknowledgements

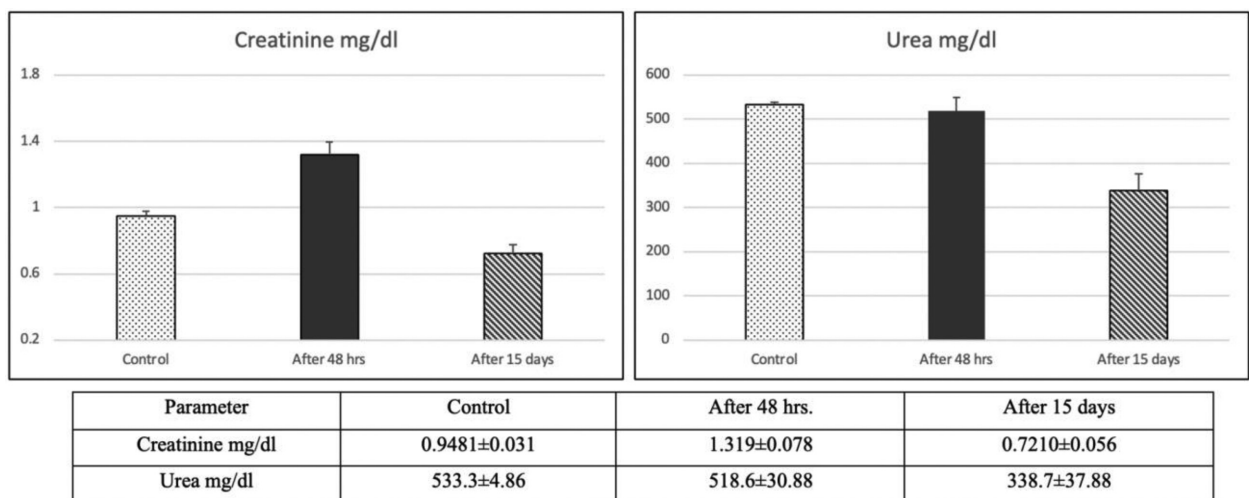
The authors acknowledge the financial support of the Science and Technology Development Fund, Egypt (STDF) administered through 'TC/2/Health/2009/

Figure 11



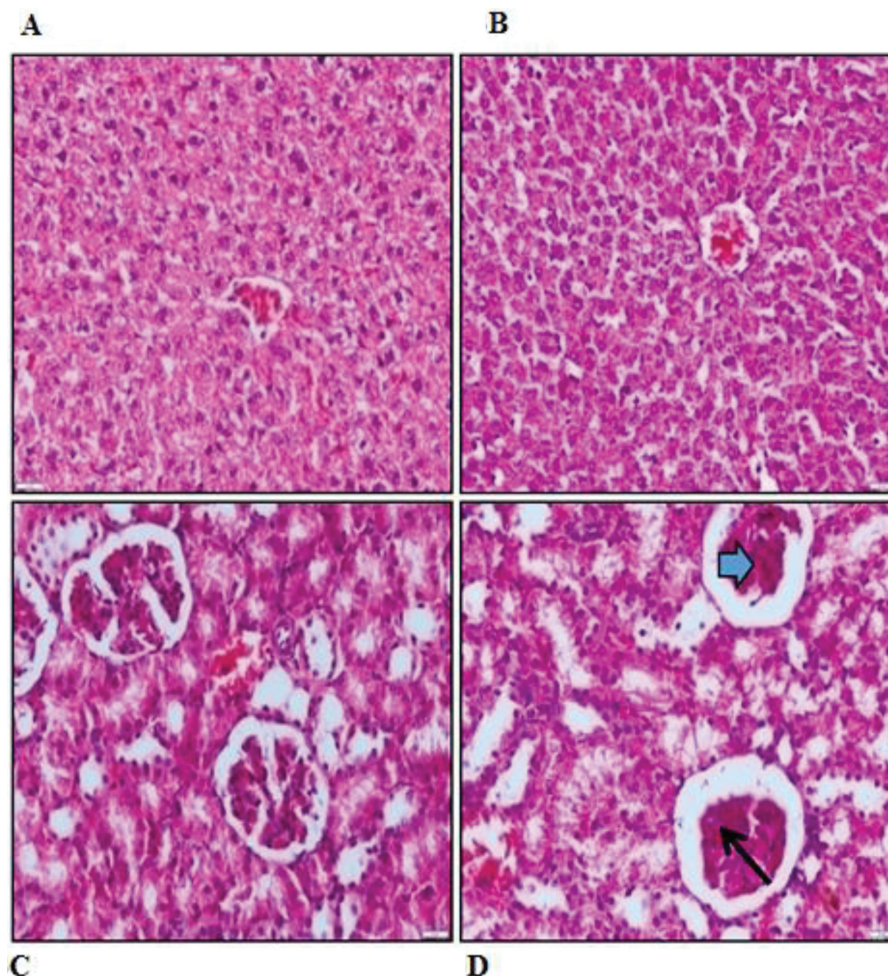
Effects of treatment with compound 12 on biochemical parameters of liver in rats (AST, ALT, and albumin). Results are expressed as mean±SEM of six rats. ALT, alanine transaminase; AST, aspartate transaminase.

Figure 12



Effects of treatment with compound 12 on biochemical parameters of kidney in rats (creatinine and urea). Results are expressed as mean±SEM of six rats.

Figure 13



(a–d) Histological observations. 13(A) Photomicrograph of liver section of normal rat showing apparently healthy hepatic parenchyma (H&E $\times 400$). 13(B) Photomicrograph of liver section of treated rat showing apparently healthy hepatic parenchyma (H&E $\times 400$). 13(C) Photomicrograph of kidneys section of normal rat showing apparently normal glomeruli and renal tubules (H&E $\times 400$). 13(D) Photomicrograph of kidneys section of treated rat showing atrophied glomerular tuft (arrow head) with degenerated renal tubules (arrow) (H&E $\times 400$).

hep-1.19: other HCV-related issues' Research Grant (STDF 1517).'

References

- Guidelines for the screening, care and treatment of persons with hepatitis C infection, World Health Organization 2014. ISBN 978 92 4 154875 5
- Guidelines for the screening, care and treatment of persons with chronic hepatitis C infection, World Health Organization 2016. ISBN 978 92 4 154961 5
- Craxi A, Laffi G, Zignego AL. Hepatitis C virus (HCV) infection: a systemic disease. *Mol Aspects Med* 2008; 29:85–95.
- Echevarria-Mayo J. Etiology and pathogenesis of viral hepatitis. *Enferm Infecc Microbiol Clin* 2006; 24:45–56.
- Bosch FX, Ribes J, Cléries R, Díaz M. Epidemiology of hepatocellular carcinoma. *Clin Liver Dis* 2005; 9:191–211.
- Chaabna K, Cheema S, Abraham A, Alrouh H, Lowenfels AB, Maisonneuve P, Mantani R. Systematic overview of hepatitis C infection in the Middle East and North Africa. *World J Gastroenterol* 2018; 24:3038–3054.
- Pham LV, Jensen SB, Fahnoe U, Pedersen MS, Tang Q, Ghanem L, *et al.* HCV genotype 1-6 NS3 residue 80 substitutions impact protease inhibitor activity and promote viral escape. *J Hepatol* 2019; 70:388–397.
- Wang G, Dyatkina N, Prhacv M, Williams C, Serebryany V, Hu Y, *et al.* Synthesis and anti-HCV activities of 4'-fluoro-2'-substituted uridine triphosphates and nucleotide prodrugs: discovery of 4'-fluoro-2'-c-methyluridine 5'-phosphoramidate prodrug (AL-335) for the treatment of hepatitis C infection. *J Med Chem* 2019; 62:4555–4570.
- Julg B, Pegu A, Abbink P, Liu J, Brinkman A, Molloy K, *et al.* Virological control by the CD4-binding site antibody n6 in simian-human immunodeficiency virus-infected rhesus monkeys. *J Virol* 2017; 91:e00498–e00517.
- Sulkowski MS, Vargas HE, Di Bisceglie AM, Kuo A, Reddy KR, Lim JK, *et al.* HCV-TARGET study group. effectiveness of simeprevir plus sofosbuvir, with or without ribavirin, in real-world patients with HCV genotype 1 infection. *Gastroenterology* 2016; 150:419–429.
- Jindracek L, Stark J. Treatment of chronic hepatitis C virus infection with crushed ledipasvir/sofosbuvir administered via a percutaneous endoscopic gastrostomy tube. *J Pharm Pract* 2018; 31:522–524.
- Tam E, Luetkemeyer AF, Mantry PS, Satapathy SK, Ghali P, Kang M, *et al.* RESCUE and ACTG A5348 study investigators. Ledipasvir/sofosbuvir for treatment of hepatitis C virus in sofosbuvir-experienced, NS5A treatment-naïve patients: findings from two randomized trials. *Liver Int* 2018; 38:1010–1021.
- Ahmed OA, Kaiser HH, Hawash N, Samir H, Shabana SST, Hassan A, *et al.* Efficacy of sofosbuvir plus ribavirin with or without peginterferon-alfa in treatment of a cohort of egyptian patients with hepatitis C virus infection. *Infect Disord Drug Targets* 2017; 17:95–100.
- Rabaan AA, Al-Ahmed SH, Bazzi AM, Alfouzan WA, Alsuliman SA, Aldrazi FA, Haque S. Overview of hepatitis C infection, molecular biology, and new treatment. *J Infect Public Health* 2020; 13:773–783.

- 15 Scotto R, Buonomo AR, Moriello NS, Maraolo AE, Zappulo E, Pinchera B, *et al.* Real-world efficacy and safety of pangenotypic direct-acting antivirals against hepatitis C Virus infection. *Rev Recent Clin Trials* 2019; 14:173–182.
- 16 Li Y, Luo G. Human low-density lipoprotein receptor plays an important role in hepatitis B virus infection. *PLoS Pathog* 2021; 17:e1009722.
- 17 Mohamed AF, Abo-Ouf AM, Arafa MAA. Histological and biochemical studies on effect of Sofosbuvir (Sovaldi) on adult male albino rat kidney. *Ultrastruct Pathol* 2021; 45:286–296.
- 18 Alazard-Dany N, Denolly S, Bosen B, Cosset FL. Overview of HCV life cycle with a special focus on current and possible future antiviral targets. *Viruses* 2019; 11:30.
- 19 Beaulieu PL, Bös M, Bousquet Y, DeRoy P, Fazal G, Gauthier J, *et al.* Non-nucleoside inhibitors of the hepatitis C virus NS5B polymerase: discovery of benzimidazole 5-carboxylic amide derivatives with low-nanomolar potency. *Bioorg Med Chem Lett* 2004; 14:967–971.
- 20 Legrand-Abravanel F, Nicot F, Izopet J. New NS5B polymerase inhibitors for hepatitis C. *Expert Opin Investig Drugs* 2010; 19:963–975.
- 21 Hirashima S, Suzuki T, Ishida T, Noji S, Yata S, Ando I, *et al.* Benzimidazole derivatives bearing substituted biphenyls as hepatitis C virus NS5B RNA-dependent RNA polymerase inhibitors: structure-activity relationship studies and identification of a potent and highly selective inhibitor JTK-109. *J Med Chem* 2006; 49:4721–4736.
- 22 Powdrill MH, Bernatchez JA, Götte M. Inhibitors of the hepatitis C Virus RNA-dependent RNA polymerase NS5B. *Viruses* 2010; 2:2169–2195.
- 23 Rong F, Chow S, Yan S, Larson G, Hong Z, Wu J. Structure-activity relationship (SAR) studies of quinoxalines as novel HCV NS5B RNA-dependent RNA polymerase inhibitors. *Bioorg Med Chem Lett* 2007; 17:1663–1666.
- 24 Horscroft N, Bellows D, Ansari I, Lai VC, Dempsey S, Liang D, *et al.* Establishment of a subgenomic replicon for bovine viral diarrhea virus in Huh-7 cells and modulation of interferon-regulated factor 3-mediated antiviral response. *J Virol* 2005; 79:2788–2796.
- 25 Whitby K, Taylor D, Patel D, Ahmed P, Tyms AS. Action of celgosivir (6-O-butanoyl castanospermine) against the pestivirus BVDV: implications for the treatment of hepatitis C. *Antivir Chem Chemother* 2004; 15:141–151.
- 26 Galal SA, Khattab M, Andreadaki F, Chrysina ED, Praly J-P, Ragab FAF, El Diwani H I. Synthesis of (benzimidazol-2-yl)aniline derivatives as glycogen phosphorylase inhibitors. *Bioorg Med Chem* 2016; 24:5423–5430.
- 27 Galal SA, Khairat SH, Ragab FA, Abdelsamie AS, Ali MM, Soliman SM, *et al.* Design, synthesis and molecular docking study of novel quinoxalin-2 (1*H*)-ones as anti-tumor active agents with inhibition of tyrosine kinase receptor and studying their cyclooxygenase-2 activity. *Eur J Med Chem* 2014; 86:122–132.
- 28 Freitag M, Schemies J, Larsen T, El Gaghlab K, Schulz F, Rumpf T, *et al.* Synthesis and biological activity of splitomicin analogs targeted at human NAD(+)-dependent histone deacetylases (sirtuins). *Bioorg Med Chem* 2011; 19:3669–3677.
- 29 Galal SA, Abdelsamie AS, Tokuda H, El Diwani HI, Part I. Synthesis and antitumor activity and molecular docking study of quinoxaline derivatives. *Eur J Med Chem* 2011; 46:327–340.
- 30 Khairat SHM, Omar MA, Ragab FAF, Roy S, Turab Naqvi AA, Abdelsamie A S, *et al.* Design, synthesis, and biological evaluation of novel benzimidazole derivatives as sphingosine kinase 1 inhibitor. *Arch Pharm (Weinheim)* 2021; 354:e2100080.
- 31 Wakita T, Pietschmann T, Kato T, Date T, Miyamoto M, Zhao Z, *et al.* Production of infectious hepatitis C virus in tissue culture from a cloned viral genome. *Nat Med* 2005; 11:791–796.
- 32 Yan S, Appleby T, Gunic E, Shim J H, Tasu T, Kim H, *et al.* Isothiazoles as active-site inhibitors of HCV NS5B polymerase. *Bioorg Med Chem Lett* 2007; 17:28–33.
- 33 Yan S, Appleby T, Larson G, Wu J Z, Hamatake R, Hong Z, Yao N, Structure-based design of a novel thiazolone scaffold as HCV NS5B polymerase allosteric inhibitors. *Bioorg Med Chem Lett* 2006; 16: 5888–5891.
- 34 Li H, Tatlock J, Linton A, Gonzalez J, Jewell T, Patel L, *et al.* Discovery of (R)-6-cyclopentyl-6-(2-(2,6-diethylpyridin-4-yl)ethyl)-3-((5,7-dimethyl-[1,2,4]triazolo[1,5-a]pyrimidin-2-yl)methyl)-4-hydroxy-5,6-dihydropyran-2-one (PF-00868554) as a potent and orally available hepatitis C virus polymerase inhibitor. *J Med Chem* 2009; 52:1255–1228.
- 35 Di Marco S. Identification of novel allosteric inhibitors of hepatitis C virus NS5B polymerase thumb domain (Site II) by structure-based design. PDB Entry - 2WRM DOI: <https://doi.org/10.2210/pdb2wrm/pdb>. To be published
- 36 Martin Hernando JI, Ontoria JM, Malancona S, Attenui B, Fiore F, Bonelli F, *et al.* Optimization of thienopyrrole-based finger-loop inhibitors of the hepatitis C virus NS5B polymerase. *Chem Med Chem* 2009; 4:1695–1713.
- 37 Le Pogam S, Kang H, Harris SF, Leveque V, Giannetti A M, Ali S, *et al.* Selection and characterization of replicon variants dually resistant to thumb- and palm-binding nonnucleoside polymerase inhibitors of the hepatitis C virus. *J Virol* 2006; 80:6146–6154.
- 38 Verdonk ML, Cole JC, Hartshorn MJ, Murray C W, Taylor RD. Improved protein-ligand docking using GOLD. *Proteins* 2003; 52:609–623.
- 39 Ijaz M, Arshad A, Awan MA, Tariq MR, Ali SW, Ali S, *et al.* Exploring the potential of curry leaves on mercury-induced hepatorenal toxicity in an animal model. *Food Sci Nutr* 2021; 10:499–506.
- 40 Weiner ID, Mitch WE, Sands JM. Urea and Ammonia Metabolism and the Control of Renal Nitrogen Excretion. *Clin J Am Soc Nephrol.* 2015; 10(8):1444–1458.
- 41 Guan Y, Nakano D, Li L, *et al.* Protease-Activated Receptor 1 Contributes to Microcirculation Failure and Tubular Damage in Renal Ischemia-Reperfusion Injury in Mice. *Biomed Res Int.* 2021;2021:6665714.
- 42 Bancroft JD, Stevens A, Turner DR. Theory and practice of histological technique. (4th ed). NY, London, San Francisco, Tokyo: Churchill Livingstone; 1996.